

1 **Cell-type specific circadian bioluminescence rhythms in *Dbp* reporter mice**

2

3 **Short Running Title:** Bioluminescence Rhythms in *Dbp* reporter mice

4

5 <sup>a,b,1</sup> Cíearra B. Smith, <sup>a,c,1</sup> Vincent van der Vinne, <sup>d</sup> Eleanor McCartney, <sup>e</sup> Adam C. Stowie, <sup>f</sup> Tanya L.

6 Leise, <sup>d,2</sup> Blanca Martin-Burgos, <sup>d</sup> Penny C. Molyneux, <sup>g</sup> Lauren A. Garbutt, <sup>h</sup> Michael H. Brodsky, <sup>e</sup> Alec

7 J. Davidson, <sup>d</sup> Mary E. Harrington, <sup>g</sup> Robert Dallmann, and <sup>a,b,i,3</sup> David R. Weaver

8

9 <sup>a</sup> Department of Neurobiology, University of Massachusetts Chan Medical School, Worcester MA

10 <sup>b</sup> Graduate Program in Neuroscience, University of Massachusetts Chan Medical School, Worcester MA

11 <sup>c</sup> Department of Biology, Williams College, Williamstown, MA

12 <sup>d</sup> Neuroscience Program, Smith College, Northampton MA

13 <sup>e</sup> Neuroscience Institute, Morehouse School of Medicine, Atlanta GA

14 <sup>f</sup> Department of Mathematics and Statistics, Amherst College, Amherst MA

15 <sup>g</sup> Division of Biomedical Sciences, Warwick Medical School, University of Warwick, Coventry, UK

16 <sup>h</sup> Department of Molecular, Cell and Cancer Biology, University of Massachusetts Chan Medical  
17 School, Worcester MA

18 <sup>i</sup> NeuroNexus Institute, University of Massachusetts Chan Medical School, Worcester MA

19

20 <sup>1</sup> C.B.S and V.v.d.V. contributed equally to this work.

21 <sup>2</sup> Present address: University of California, San Diego, La Jolla, CA USA

22 <sup>3</sup> To whom correspondence may be addressed:

23 Email: [David.weaver@umassmed.edu](mailto:David.weaver@umassmed.edu)

24 David R. Weaver, Ph.D., Department of Neurobiology, LRB-723, UMass Medical School, 364

25 Plantation St., Worcester MA 01605

26 **Keywords:** Circadian Rhythms, Bioluminescence, Luciferase, Misalignment, *Dbp*, Albumin D-element  
27 binding protein, *In Vivo* Imaging System (IVIS), LumiCycle *In Vivo*, Reporter Mouse, Peripheral  
28 Oscillators

29 **Conflict of interest statement:** The authors declare no conflicts of interest.

30 **Abstract**

31 Circadian rhythms are endogenously generated physiological and molecular rhythms with a cycle length  
32 of about 24 h. Bioluminescent reporters have been exceptionally useful for studying circadian rhythms in  
33 numerous species. Here, we report development of a reporter mouse generated by modification of a  
34 widely expressed and highly rhythmic gene encoding D-site albumin promoter binding protein (*Dbp*). In  
35 this line of mice, firefly luciferase is expressed from the *Dbp* locus in a *Cre*-recombinase-dependent  
36 manner, allowing assessment of bioluminescence rhythms in specific cellular populations. A mouse line  
37 in which luciferase expression was *Cre*-independent was also generated. The *Dbp* reporter alleles do not  
38 alter *Dbp* gene expression rhythms in liver or circadian locomotor activity rhythms. *In vivo* and *ex vivo*  
39 studies show the utility of the reporter alleles for monitoring rhythmicity. Our studies reveal cell-type  
40 specific characteristics of rhythms among neuronal populations within the suprachiasmatic nuclei *ex vivo*.  
41 *In vivo* studies show *Dbp*-driven bioluminescence rhythms in the liver of *Albumin-Cre;Dbp<sup>KI/+</sup>* “liver  
42 reporter” mice. After a shift of the lighting schedule, locomotor activity achieved the proper phase  
43 relationship with the new lighting cycle more rapidly than hepatic bioluminescence did. As previously  
44 shown, restricting food access to the daytime altered the phase of hepatic rhythmicity. Our model allowed  
45 assessment of the rate of recovery from misalignment once animals were provided with food *ad libitum*.  
46 These studies confirm the previously demonstrated circadian misalignment following environmental  
47 perturbations and reveal the utility of this model for minimally invasive, longitudinal monitoring of  
48 rhythmicity from specific mouse tissues.

49

## 50 **Introduction**

51 Circadian rhythms are endogenous rhythms with a cycle length of ~24 hours. The mammalian  
52 circadian system is hierarchical, with the hypothalamic suprachiasmatic nuclei (SCN) serving as the  
53 pacemaker (Mohawk et al., 2012; Herzog et al., 2017). The SCN are synchronized by environmental cues,  
54 of which the light-dark cycle is the most influential. The SCN are not unique in their capacity for  
55 rhythmicity, however. The transcriptional-translational feedback loop regulating molecular oscillations in  
56 the SCN is also present in individual cells throughout the body (Mohawk et al., 2012). SCN-driven  
57 neural, behavioral and hormonal rhythms synchronize these cell-autonomous oscillators, leading to  
58 rhythmicity with predictable phase relationships among tissues, genes and physiological processes  
59 (Mohawk et al., 2012; Patke et al., 2020; Zhang et al., 2014). Repeated disruption of this internal temporal  
60 order by inappropriately timed light exposure or food intake leads to adverse health consequences in shift-  
61 working humans and in animal models (Evans & Davidson, 2013; Patke et al., 2020). Progress in  
62 identifying the mechanisms by which chronic circadian disruption leads to adverse health consequences  
63 will require long-term monitoring of central and peripheral rhythms (Roenneberg & Merrow, 2016).

64 Rhythmically expressed reporter genes have been extremely important for demonstrating cell-  
65 autonomous circadian clocks and monitoring rhythmicity in several organisms, including plants (Millar et  
66 al., 1992), *Neurospora* (Morgan et al., 2003), cyanobacteria (Kondo et al., 1993), *Drosophila* (Brandes et  
67 al., 1996), zebrafish (Weger et al., 2013), cultured cells (Nagoshi et al., 2004; Hirota et al., 2010; Welsh et  
68 al., 2004; Zhang et al., 2009), rodent tissue explants (Abe et al., 2002; Maywood et al., 2013; Yamazaki et  
69 al., 2000; Yoo et al., 2004; Yoo et al., 2005), and rodent tissues *in vivo* (Saini et al., 2013; Tahara et al.,  
70 2012). Circadian reporter genes have been instrumental in screens to identify clock genes and modifiers in  
71 many of these systems (Cesbron et al., 2013; Chen et al., 2012; Hirota et al., 2010; Kondo et al., 1993;  
72 Millar et al., 1995; Muñoz-Guzmán et al., 2021; Stanewsky et al., 1998; Zhang et al., 2009). Circadian  
73 reporters have also been used to assess rhythmicity in peripheral tissues and the impact of alterations in  
74 experimental or environmental conditions (food availability, lighting cycles, glucocorticoid treatment) on  
75 peripheral oscillators, conducted by measuring bioluminescence rhythms in tissue explants monitored *ex*

76 *vivo* (Davidson et al., 2008; Davidson et al., 2009; Nakamura et al., 2005; Pezuk et al., 2012; Sellix et al.,  
77 2012; Stokkan et al., 2001; Yamanaka et al., 2008; Yamazaki et al., 2000). These studies complement  
78 work done by assessing population rhythms in gene expression in tissue samples indicating altered  
79 rhythm amplitude and phase, and altered phase relationships in and between SCN and peripheral  
80 oscillators following resetting (Balsalobre et al., 2000; Damiola et al., 2000; Destici et al., 2013; Nagano  
81 et al., 2003; Reddy et al., 2002; Yamaguchi et al., 2013; for review see Nicholls et al., 2019). Several  
82 groups have developed methods for *in vivo* assessment of reporter gene activity from brain regions,  
83 including the SCN, using implanted optical fibers and freely moving (but tethered) rodents (Hamada et  
84 al., 2016; Mei et al., 2018; Nakamura et al., 2008; Ono et al., 2015; Yamaguchi et al., 2001; Yamaguchi  
85 et al., 2016). Other studies have localized the source of bioluminescence from widely expressed reporter  
86 genes in specific peripheral tissues based on photomultiplier tube placement on the body surface (Hamada  
87 et al., 2016; Sawai et al., 2019). Peripheral organ reporter gene activity has been assessed by *in vivo*  
88 imaging in anesthetized mice (Saini et al., 2013; Tahara et al., 2012) and more recently in ambulatory  
89 mice (Martin-Burgos et al., 2020; Saini et al., 2013; Sinturel et al., 2021). In some cases, viral vectors  
90 that afford anatomical specificity (through their site of injection, tropism and/or by their design) have  
91 been used to direct reporter expression to specific tissues (Mei et al., 2018; Saini et al., 2013; Sinturel et  
92 al., 2021). All of these approaches are hampered by the need to develop specific reagents or approaches  
93 for each tissue being examined, and many of these approaches are invasive. In view of the large number  
94 of mouse lines with tissue-specific expression of Cre recombinase, the field would benefit considerably  
95 from a binary (Cre-lox) reporter system in which bioluminescence from a rhythmically expressed gene  
96 can be switched on in tissues expressing Cre recombinase, simply by crossing mice of the appropriate  
97 genotypes together.

98         Here, we report a new transgenic mouse line in which firefly luciferase is expressed from the  
99 mouse *Dbp* locus in a Cre-recombinase-dependent manner. *Dbp* is widely and rhythmically expressed  
100 (Fonjallaz et al., 1996; Punia et al., 2012; Zhang et al., 2014), allowing detection of circadian  
101 bioluminescence rhythms in numerous tissues, *in vivo* and *ex vivo*. Cre-dependent bioluminescence

102 rhythms were recorded *ex vivo* from specific SCN neuronal populations. Furthermore, we observed  
103 transient misalignment between behavioral and hepatic bioluminescence rhythms in freely moving mice  
104 subjected to a shift of the light-dark cycle or following restricted food access.

105 While this work was being prepared for publication, Shan et al. (2020) reported development of a  
106 Color-Switch *Per2* reporter mouse. In this reporter, Cre recombinase expression changes the reporter  
107 fused to mPER2 from red to green luciferase.

108

## 109 **Materials and Methods**

110

### 111 **Animals and Housing Conditions**

112 All animal procedures were reviewed and approved by the Institutional Animal Care and Use  
113 Committees of the University of Massachusetts Medical School, Morehouse School of Medicine, the  
114 University of Warwick, and/or Smith College.

115 Unless otherwise noted, animals were maintained in a 12h light: 12h dark (LD) lighting cycle  
116 with access to food (Prolab Isopro RMH3000; LabDiet) and water available *ad libitum*. Zeitgeber Time  
117 (ZT) refers to time relative to the lighting cycle. ZT 0-12h is the light phase and ZT 12-24h is the dark  
118 phase.

119 *Cre* recombinase-expressing lines were crossed to mice bearing the conditional (*Dbp<sup>KI</sup>*) reporter  
120 allele to generate mice expressing luciferase in specific cells or tissues. *Albumin-Cre* (B6.Cg-*Speer6-*  
121 *ps1<sup>Tg(Alb-Cre)21Mgn/J</sup>*; JAX stock number 003574), *Ksp1.3-Cre* (B6.Cg-Tg{*Cdh16-cre*}911gr/J, JAX  
122 012237), *AVP-IRES2-Cre* (B6.Cg-*Avp<sup>im1.1(Cre)Hze</sup>*/J; JAX 023530), and *NMS-Cre* mice and *NMS-Cre*  
123 (*Tg(Nms-iCre)<sup>20Ywa</sup>*, JAX 027205) were obtained from the Jackson Labs (Bar Harbor, ME). These lines  
124 direct Cre recombinase expression to hepatocytes (Postic et al., 1999), renal tubules and genito-urinary  
125 epithelia (Shao et al., 2002), neurons expressing arginine vasopressin (AVP; Harris et al., 2014), and  
126 neurons expressing Neuromedin S (NMS; Lee et al., 2015), respectively. A *Prrxl-Cre* female (B6.Cg-

127 Tg(Prrx1-Cre<sup>1Cj</sup>/J), JAX 005584; Logan et al., 2002) was used for germline deletion of the conditional  
128 allele (see below).

129 Founder *Per2*<sup>LucSV/+</sup> mice with an in-frame fusion of firefly luciferase to PER2 and an SV40  
130 polyadenylation signal (Welsh et al., 2004; Yoo et al., 2017) were generously provided by Dr. Joseph  
131 Takahashi, University of Texas Southwestern Medical School, Dallas. All *Per2*<sup>LucSV</sup> reporter mice used for  
132 experiments here were heterozygous (e.g., *Per2*<sup>LucSV/+</sup>). For clarity when referring to literature describing  
133 the more widely used *PER2::LUCIFERASE* fusion reporter line in which the endogenous *Per2* 3' UTR is  
134 downstream of the luciferase coding sequence (Yoo et al., 2004), we will refer to this line as *Per2*<sup>Luciferase</sup>.  
135 Mouse lines were maintained by backcrossing to the C57BL/6J (JAX 000664) background.

136 We also generated albino reporter mice by backcrossing to albino C57BL/6J mice with a  
137 mutation in tyrosinase (*tyr/tyr*; B6(Cg)-*Tyr*<sup>c-2J</sup>/J, JAX stock number 00058). Tyrosinase, like *Dbp*, is  
138 located on mouse chromosome 7. Crossing these lines eventually generated a recombinant (*Dbp*<sup>KI/+</sup>;  
139 *tyr/tyr*) in which both mutant alleles were on the same chromatid. Subsequent crossing to albino mice  
140 expressing Cre recombinase allowed production of albino reporter mice.

141 Note, caution is needed with the *Ksp1.3-Cre* line reported here, as it has a high frequency of  
142 germline recombination (excision of the floxed region of the conditional allele in the germline, leading to  
143 non-conditional luciferase expression) when *Ksp1.3-Cre* is present in the same parent as *Dbp*<sup>KI/+</sup>.  
144 Recombination also frequently occurs when *Ksp1.3-Cre* females are crossed with *Dbp*<sup>KI</sup> males. When  
145 using the *Cre/lox* system, genotyping strategies should be designed to detect all possible alleles. Even  
146 when the *Ksp1.3-Cre; Dbp*<sup>KI/+</sup> genotype is generated without germline excision of GFP, the sex difference  
147 in *Cre* expression leads to markedly different bioluminescence patterns in males and females (see  
148 Results).

149

### 150 **CRISPR/Cas9 targeting the *Dbp* locus**

151 The mutant allele was generated by CRISPR/Cas9 mediated engineering of the *Dbp* locus. The  
152 targeting construct (**Figure 1**) consisted of a 5' homology arm terminating just 5' of the *Dbp* stop codon

153 followed by in-frame sequences encoding a T2A linker (to separate DBP protein from the reporter  
154 polypeptides; Kim et al., 2011), LoxP, GFP with the bovine growth hormone polyadenylation signal,  
155 LoxP, and Luc2 followed by the 3'-UTR of *Dbp* (3' homology arm). In the presence of Cre recombinase,  
156 two loxP sites oriented in the same direction will recombine, leading to deletion of the sequence between  
157 them (GFP in this case).

158 In the successful set of microinjections, 34 blastocysts were injected with 40 ng/ $\mu$ l guide RNA  
159 MmDBPki\_gR49f, 50 ng/ $\mu$ l *Cas9* mRNA (synthesized from a *Cas9* PCR product using mMessage  
160 mMachinE T7 Ultra Kit from Life Technologies) and 20 ng/ $\mu$ l CAS9 protein (IDT). Two putative  
161 founders were identified using a primer pair internal to the construct (primer pair C; **Table S1**).  
162 Additional primer pairs consisting of a primer in flanking DNA (external to the construct) and a primer  
163 within the construct were used to determine whether these animals had the desired targeting event (primer  
164 pairs F and H, which spanned the 5' and 3' ends, respectively). These studies led to identifying one mouse  
165 as having the correct insertion and recognizing that the other putative founders had random insertion of  
166 the construct rather than homologous recombination into the *Dbp* locus; the mouse with random insertion  
167 was not studied further. Genomic DNA from the founder with insertion into the *Dbp* locus was amplified  
168 using a primer pair flanking the entire construct. Sequencing the product confirmed the construct was  
169 inserted properly, *in vivo*. Primer sets used for verification of the proper insertion of the construct are  
170 listed in **Table S1**.

171 The founder carrying the targeted (knock-in or *Dbp*<sup>KI</sup>) allele and its offspring were backcrossed to  
172 C57BL/6J mice (JAX 000664) for three generations before any intercrossing to reduce the chance of a  
173 potential off-target mutations becoming established in the reporter line.

174 To generate mice with germline deletion of GFP (and thus leading to expression of luciferase  
175 throughout the body), a male *Dbp*<sup>KI/+</sup> was bred to a *Prrx1-Cre* female, which we had on hand and which,  
176 in our experience, produces germline deletion of floxed alleles at high frequency when Cre is introduced

177 from the female. Several mice bearing the newly generated  $Dbp^{Luc}$  allele were identified and backcrossed  
178 to C57BL/6J mice, selecting against *Prrx1-Cre*.

179

## 180 **Genotyping**

181 Genotyping was performed by PCR amplification of DNA extracted from ear punches.  
182 Amplification products were separated by agarose gel electrophoresis. Genotyping protocols for  $Per2^{LucSV}$   
183 and *Cre* recombinase have been published previously and are listed in Table S1 (van der Vinne et al.,  
184 2018; Weaver et al., 2018, respectively). A mixture of four primers (primer set “4A”) capable of detecting  
185 all possible *Dbp* allele combinations was used for colony genotyping; the three possible alleles ( $Dbp^{KI}$ ,  
186  $Dbp^{Luc}$ ,  $Dbp^{+}$ ) generate amplicons of 399, 490 and 299 bp, respectively with this primer set. Primer set  
187 4A consists of a common forward primer in exon 4 (5'-TGCTGTGCTTTCACGCTACCAGG-3') and  
188 allele-specific reverse primers in GFP (to detect the  $Dbp^{KI}$  allele; 5'-  
189 AGTCGTGCTGCTTCATGTGGTCG-3'), in *Luc2* (to detect the  $Dbp^{Luc}$  allele; 5'-  
190 TCGTTGTAGATGTCGTTAGCTGG-3'), and in the *Dbp* 3' UTR (to detect the unmodified *Dbp* allele;  
191 5'-TTCAGGATTGTGTTGATGGAGGC-3').

192

## 193 **Generation of Digoxigenin (DIG) DNA Probes and Northern Blot Assay.**

194 DIG-labeled DNA probes were generated by PCR in reactions containing 28  $\mu$ M of DIG-labeled  
195 UTP. Primer sets are listed in **Table S1**.

196 Male mice of five genotypes (WT,  $Dbp^{KI/+}$ ,  $Dbp^{KI/KI}$ ,  $Dbp^{Luc/+}$ , and  $Dbp^{Luc/Luc}$ ) were euthanized by  
197 Euthasol injection for collection of liver tissue at 4-h intervals (ZT 2, 6, 10, 14, 18, 22). RNA was isolated  
198 from the liver tissue by Trizol extraction (Ambion). RNA was quantitated by Nanodrop. Five micrograms  
199 per lane were separated by electrophoresis on 1.2% formaldehyde gels. RNA was transferred to nylon  
200 membranes and cross-linked by UV exposure. Blots were prehybridized, probed and detected following  
201 the manufacturer's protocol (Roche), bagged and exposed to X-ray film.



202 Film images of the blots were analyzed by determining the optical density of the *Dbp* and *Actin*  
203 bands within each lane and taking the *Dbp/Actin* ratio. The *Dbp/Actin* ratios were converted to  
204 percentage of maximum *Dbp/Actin* for each transcript type within each blot. Due to the difference in band  
205 location of the three *Dbp* alleles, heterozygous animals contributed a set of values for both the wild-type  
206 transcript and the reporter transcript on each blot. Friedman's one-way analysis of variance and Dunn's  
207 test were used for non-parametric assessment of differences between time-points for each transcript.

208

### 209 **Locomotor Activity Rhythms**

210 Male and female mice of five genotypes (WT, *Dbp*<sup>KI/+</sup>, *Dbp*<sup>KI/KI</sup>, *Dbp*<sup>Luc/+</sup>, and *Dbp*<sup>Luc/Luc</sup>) were  
211 transferred to the experimental room and single-housed with a running wheel. Animals had access to food  
212 and water *ad libitum*. Running-wheel activity was monitored and analysed using ClockLab collection  
213 software (Actimetrics). Mice were entrained to a 12-h light/12-h dark cycle for 18 days, then were placed  
214 into constant darkness (dim red light) for 15 days. The free-running period in constant darkness (DD) was  
215 determined for each animal on DD days 4-15 by periodogram analysis (ClockLab).

216

### 217 **Bioluminescence Recordings from Tissue Explants**

218 Tissue explants were prepared late in the afternoon from *Per2*<sup>LucSV/+</sup> and *Dbp*<sup>Luc/+</sup> mice housed on  
219 a 12-h light/12-h dark lighting cycle. Tissues from the two genotypes were studied together in each run.  
220 Mice were deeply anesthetized with Euthasol and decapitated. Tissues were dissected and immediately  
221 placed in ice-cold 1X HBSS (Gibco). Pituitary gland was subdivided into 4 sections (~2mm<sup>3</sup>) with a  
222 scalpel and each piece was cultured separately. Lung explants were placed three per dish. Up to three  
223 replicate dishes were studied per tissue per animal. Explants were placed on sterile 35-mm Millicell  
224 culture plate inserts (Millipore) in a sealed petri dish containing air-buffered bioluminescence medium  
225 (Yamazaki and Takahashi, 2005) plus D-luciferin (100 μM) (Gold Biotechnology) and incubated at 32 °C  
226 as previously described (van der Vinne et al., 2018). Bioluminescence in each dish was measured for 1  
227 minute every 15 minutes using a Hamamatsu LM-2400 luminometer.

228 Bioluminescence records were analyzed using Microsoft Excel to determine period and peak  
229 time. The first 12-h were discarded to exclude acute responses to explant preparation. Photon counts were  
230 smoothed to a 3-h running average and baseline subtracted using a 24-h running average. Circadian  
231 period was determined from the average of the period between each peak, trough, upward crossing and  
232 downward crossing between 24 and 88 hr of recording for each record. Peak time was calculated as the  
233 clock time of the first peak in the background-subtracted data and is expressed relative to ZT of the  
234 extrapolated lighting cycle.

235

### 236 **Imaging of Bioluminescence Rhythms *In Vivo***

237 *In vivo* imaging was performed in the UMass Medical School Small Animal Imaging Core  
238 Facility using an *In Vivo* Imaging System (IVIS-100, Caliper, now Perkin Elmer) as previously described  
239 (van der Vinne et al., 2018; van der Vinne et al., 2020). *Alb-Cre*<sup>+</sup>; *Dbp*<sup>KL/+</sup> (liver reporter), *Dbp*<sup>Luc/+</sup>, and  
240 *Per2*<sup>LucSV/+</sup> mice were anesthetized with 2% isoflurane (Zoetis Inc.) and skin covering the liver, kidneys  
241 and submandibular glands was shaved. Mice were injected with D-luciferin (i.p., 100 µl at 7.7 mM, Gold  
242 Biotechnology) and dorsal (9 min post-injection) and ventral (10.5 min post-injection) images were  
243 captured. To assess bioluminescence rhythms, anesthesia, D-luciferin injection and imaging was repeated  
244 at 4- to 8-hour intervals over approximately 30 hours. IVIS images were analyzed using Caliper Life  
245 Sciences' Living Image software (version 4.4) within Regions of Interest (ROI) of fixed size.

246 Whole-body reporters (*Dbp*<sup>Luc/+</sup>) and liver reporters (*Alb-Cre*<sup>+</sup>; *Dbp*<sup>KL/+</sup>) were also used to assess  
247 the distribution of bioluminescence by IVIS imaging. Mice were anesthetized with isoflurane, shaved,  
248 and injected with D-luciferin (100 microliters at 7-10 mM, i.p.) at times of peak expression (ZT 11-16).  
249 Images were captured of ventral and dorsal views at 9-12 minutes after injection. Bioluminescent counts  
250 within regions of interest (ROIs) were calculated using Living Image software. ROIs identified on the  
251 ventral surface were the whole rectangular region containing the mouse, and sub-ROI's were a region in  
252 the throat (submandibular gland), upper abdomen, and lower abdomen. Dorsal ROI's were the rectangle

253 containing the entire mouse and a sub-ROI over the lower back, corresponding to the abdomen on the  
254 dorsal side. Subsequent calculations were performed in Microsoft Excel.

255 Liver reporter mice were euthanized and dissected to confirm that bioluminescence originated  
256 exclusively from the liver. In *Per2<sup>LucSV</sup>* mice, major sources of bioluminescence in the abdomen were  
257 liver, kidney and intestines (see also Martin-Burgos et al., 2020).

258

### 259 **Bioluminescence Imaging of SCN Explants**

260 Coronal sections containing SCN from adult *NMS-Cre;Dbp<sup>KI/+</sup>*, *AVP-IRES-CRE;Dbp<sup>KI/+</sup>*, and  
261 *Dbp<sup>Luc/+</sup>* mice were dissected, cultured, and imaged as previously described (Evans et al., 2011; Evans et  
262 al., 2013). Briefly, sections containing SCN (150  $\mu$ m) were cultured on a Millicell membrane in air-  
263 buffered media containing 100  $\mu$ M D-luciferin (Gold Biotechnology) and imaged for 5 days using a  
264 Stanford Photonics XR/MEGA-10Z cooled intensified charge-coupled device camera.

265 Rhythmic parameters of luciferase expression were calculated for each slice and for cell-like  
266 regions of interest (ROIs) within each slice using computational analyses in MATLAB (R2018a,  
267 MathWorks) as described previously (Evans et al., 2013; Leise & Harrington, 2011). Briefly, to  
268 locate and extract data from cell-like ROIs, we employed an iterative process identifying clusters of at  
269 least 20 bright pixels after background and local noise subtraction (through application of a 2D wavelet  
270 transform using Wavelab 850, (<https://statweb.stanford.edu/~wavelab/>) of a slice image summed across  
271 24 h of bioluminescence. To extract time series for the ROI's, each image in the sequence was smoothed  
272 via convolution with a Gaussian kernel applied to 12x12-pixel regions and reduced from 512x640  
273 resolution to 256x320. A discrete wavelet transform (DWT) was applied to each time series to remove the  
274 trend and to extract the circadian and noise components using the *wmtsa* toolbox for MATLAB  
275 (<https://atmos.uw.edu/~wmtsa/>). The criteria for circadian rhythmicity in the ROI time series were a peak  
276 autocorrelation coefficient of at least 0.2, a circadian component peak-to-peak time between 18 and 30 h,  
277 an amplitude above baseline noise (standard deviation of noise component), and a cross-correlation

278 coefficient of at least 0.4 with an aligned sine wave over a 48h window. Peaks of the DWT circadian  
279 component were used to estimate peak time of each ROI.

280 Rhythmicity index (RI) is the peak in the autocorrelation of the DWT-detrended time series,  
281 corresponding to a lag between 16 and 36 hrs, as previously described (Leise et al., 2013; Leise, 2017).  
282 The time of peak bioluminescence, rhythmicity index and the scatter of peak times within each slice for  
283 each ROI was assessed on the first day *ex vivo*. Period of rhythmicity in each ROI was determined as the  
284 average peak-to-peak interval in the second and third cycles. These measures were compared between  
285 genotypes by a general linear model, with slice ID included as a random variable to account for multiple  
286 cells being measured on each slice. Where applicable, post-hoc comparisons were performed using  
287 Tukey's HSD pairwise comparisons.

288

## 289 **Data Collection and Analysis of Bioluminescence Rhythms in Ambulatory Liver Reporter Mice**

290 Bioluminescence was measured in freely moving *Alb-Cre<sup>+</sup>; Dbp<sup>KI/+</sup>* reporter mice with the  
291 “Lumicycle *In Vivo*” system (Actimetrics, Wilmette, IL) using methods as recently described (Martin-  
292 Burgos et al., 2020). Animals were checked daily at varied times using an infrared viewer (Carson  
293 OPMOD DNV 1.0), or goggles (Pulsar Edge Night Vision Goggles PL75095).

294 Each Lumicycle *In Vivo* unit contained two PMTs (Hamamatsu H8259-01), and programmable  
295 LED lights. A programmable shutter blocked the PMTs during periods of light exposure and to measure  
296 ‘dark counts’. Each 1-minute dark-count value was subtracted from the counts recorded during the  
297 subsequent 14 minutes to obtain the background-corrected count values, to compensate for the effect of  
298 temperature fluctuations on PMT signal.

299 Ambulatory bioluminescence data were analyzed using RStudio. A discrete wavelet transform  
300 (DWT) was applied to each time series to detrend and to calculate the time of peaks using the *wmtsa* R  
301 package (<https://cran.r-project.org/web/packages/wmtsa/index.html>), as described (Leise & Harrington,  
302 2011; Leise et al., 2013; Leise, 2017). The S12 filter was applied on 15-min median binned data; medians

303 were used (instead of means) to reduce the effect of large outliers. Data before the first trough and after  
304 the last trough were discarded to avoid edge effects.

305 Locomotor activity was recorded using passive infrared motion sensors (Viconic, K940) and  
306 Clocklab software (RRID:SCR\_014309). The mid-point of locomotor activity was determined by  
307 wavelet analysis on each day of recording. Midpoints were used because the onset of locomotor activity  
308 is poorly defined using motion sensors (relative to running wheel onsets).

309

### 310 **Assessing Routes of Administration of Luciferin.**

311 To determine whether rhythmic substrate intake influences the pattern of bioluminescence, we  
312 compared the time of peak bioluminescence between animals receiving continuous administration of  
313 substrate (from a subcutaneous osmotic minipump) with trials in which mice received D-luciferin in the  
314 drinking water (2 mM) and implantation of a PBS-filled osmotic pump.

315 Liver reporter mice previously housed in 12L:12D were entrained to a skeleton photoperiod  
316 (SPP) consisting of four 1-hour light pulses. A skeleton photoperiod provides additional periods of  
317 darkness in which to record bioluminescence. The use of a 4-pulse SPP (rather than the more typical 2-  
318 pulse SPP) was based on preliminary studies indicating a 4-pulse SPP could more consistently cause  
319 phase advances of locomotor activity following an advance shift of the lighting cycle. In this 4-pulse SPP,  
320 illumination occurred in four 1-hour blocks within the light phase in the preceding lighting cycle (e.g.,  
321 lights were on from ZT 0-1, 2-3, 9-10, and 11-12, so the first and last hours of light in SPP coincided with  
322 the first and last hours of illumination in the full photocycle (with lights on ZT0-12 and lights off ZT12-  
323 24/0).

324 On the seventh day of SPP entrainment, mice were given analgesics (0.05 mg/kg Buprenorphine  
325 and 2.0 mg/kg Meloxicam), anesthetized with 3% isoflurane, shaved from hips to shoulders, and a primed  
326 osmotic minipump (Alzet Model #1002, 0.25 $\mu$ l per hour, 14 day) containing D-luciferin (100 mM  
327 dissolved in PBS) or PBS vehicle was implanted subcutaneously. Mice were returned to their cages with a  
328 warming disc and were provided soft food during the first 24 hours of recovery. Animals were placed into

329 the LumiCycle *In Vivo* unit 2.5 days after surgery. Bioluminescence was recorded in SPP lighting for 2.5  
330 days, then lights were disabled at the time of lights-out. The time of peak bioluminescence was  
331 determined by wavelet analysis on the first day in constant darkness. No difference in peak time of  
332 bioluminescence was found (see Results); in subsequent studies of ambulatory Liver reporter mice, D -  
333 luciferin (2 mM) was administered in the drinking water.

334

### 335 **Re-entrainment following a Phase Shift of the Skeleton Photoperiod.**

336 Liver reporter mice (*Albumin-Cre; Dbp<sup>KI/+</sup>*) previously entrained to LD were transferred to the  
337 skeleton photoperiod for several days. Mice were anesthetized with isoflurane and shaved 2.5 days prior  
338 to placement in the LumiCycle *In Vivo* units. D-Luciferin (2 mM) was provided in the drinking water.  
339 Skeleton photoperiod lighting conditions were either maintained at the initial pattern or advanced by 6 hr  
340 after the second day of recording. Locomotor activity was detected by passive infrared motion sensors.

341 The circadian time of peak bioluminescence and the mid-point of locomotor activity were  
342 determined by wavelet analysis on each day of recording. We used the midpoint of locomotor activity  
343 because activity onset was not easily defined using motion sensors. The timing of bioluminescence and  
344 locomotor activity rhythms was normalized to the timing of these rhythms on Day 2 (e.g., the last day  
345 before shifting the lighting cycle in the shifted group) for each animal. Data are expressed as mean  $\pm$   
346 SEM for each lighting condition and endpoint on each day. Data from each lighting group were analyzed  
347 separately using a general linear model with Animal ID as a random variable (allowing comparison of the  
348 two rhythms within individuals) and the main effects of the endpoint measure (locomotor activity or  
349 bioluminescence) and Day number, and the 2-way interaction Measure\*Day. In animals not undergoing a  
350 phase shift, potential changes in the timing of the locomotor or bioluminescence rhythm were assessed  
351 separately for either measure by testing the influence of Day number.

352

### 353 **Food Restriction Followed by Bioluminescence Recording.**

354 Liver reporter mice (*Albumin-Cre; Dbp<sup>KI/+</sup>*) were fed pellets (300 mg, Dustless Precision Pellets,  
355 Rodent, Grain-Based, F0170, BioServ, Flemington, NJ, USA) through the Actimetrics timed feeding  
356 apparatus designed by Phenome Technologies, Skokie, IL, USA. Pellets were spaced by a minimum of 10  
357 minutes to prevent hoarding behaviour (Acosta-Rodriguez et al., 2017). Liver reporter animals were  
358 randomly assigned to treatment groups and recording boxes. Three groups were studied: those with *ad*  
359 *libitum* access to food, those with feeding restricted to the light phase of the LD cycle (daytime feeding),  
360 and mice with access to food restricted to the dark phase of the LD cycle (nighttime feeding). Mice were  
361 weighed regularly to ensure body weight did not decrease below 95% of initial weight. All mice were  
362 kept on a 12L:12D lighting schedule during the period of food manipulation, and then were released into  
363 constant darkness with D-luciferin (2mM) in the drinking water for bioluminescence recording. During  
364 the LD period, data were collected on feeding, light levels, and locomotor behavior (using motion  
365 sensors). Three days before entering the LumiCycle *In Vivo* units, cage bottoms were changed at dark  
366 onset. *Ad libitum* and night-fed mice were placed into the LumiCycle *In Vivo* units at dark onset with food  
367 immediately available. Day-fed mice were placed into the LumiCycle *In Vivo* units at dark onset but were  
368 provided food after 12 hours (at the time of light onset in the previous LD cycle) to continue the daytime  
369 feeding regime during the first day of the recording period. Bioluminescence was recorded for 7 days.

370 Experimental groups and controls ran in parallel over five cohorts lasting 3 months. 24 hours  
371 prior to placement in the recording boxes, mice were shaved from hips to shoulders on their front and  
372 back under 3% isoflurane and returned to their cages. Mice were provided with D-luciferin (2mM) in the  
373 drinking water 6 hours prior to placement into the LumiCycle *In Vivo* units, to enable instantaneous  
374 bioluminescence upon recording onset.

375 The center of gravity (COG) of food intake was calculated for each animal for the last 5 days in  
376 LD (e.g., the last 5 days of the feeding regimen). Food intake patterns were also independently assessed  
377 qualitatively by four observers. These assessments led to identification of three cohorts of mice, based on  
378 food intake patterns. Three mice were identified as clear outliers compared to these three cohorts based on  
379 visual inspection of the food intake timing. In line with this qualitative assessment, the feeding COG of

380 each of these 3 animals was >2 h removed from the other animals in their cohort (**Fig. 7C**). These three  
381 animals were excluded from cohort-based assessments. Peak of bioluminescence on each day was  
382 calculated by DWT analysis as above. Missing data resulted from inability to define a time of peak  
383 bioluminescence on some days. Hair regrowth contributed to loss of signal and loss of rhythm amplitude,  
384 and thus to missing data in some cases.

### 385 **Data and Materials Availability**

386 Requests for research materials should be directed to Dr. David Weaver. Underlying data are  
387 available from Dr. Weaver on request.

388

### 389 **Results**

390 **Generation of a bifunctional reporter mouse.** CRISPR/Cas9 genome editing was used to introduce a  
391 bifunctional reporter into the mouse *Dbp* locus (**Fig. 1**). The reporter consists of a T2A sequence (to allow  
392 expression of separate proteins from a single transcript), a destabilized, enhanced GFP (d2EGFP,  
393 hereafter GFP) sequence flanked by loxP sites, and a codon optimised synthetic firefly *luciferase* (*Luc2*  
394 from *Photinus pyralis*, hereafter *luc*). In the absence of *Cre* expression, DBP and GFP are expressed as  
395 separate proteins. After CRE-mediated recombination, the floxed GFP is removed, and separate DBP and  
396 luciferase proteins are expressed from the *Dbp* locus. Sequencing of genomic DNA confirmed successful  
397 generation of the *Dbp<sup>KI</sup>* conditional reporter allele.

398 A non-conditional reporter allele was generated by breeding to combine the conditional *Dbp<sup>KI</sup>*  
399 allele with *Cre*-recombinase expressed in the germline (of a female *Prrx1-Cre* mouse), leading to  
400 germline excision of GFP. We refer to this non-conditional allele, which has the potential to express  
401 luciferase wherever *Dbp* is expressed, as *Dbp<sup>Luc</sup>*.

402

403 **Molecular and Behavioral Rhythms in Mice with *Dbp* Reporter Alleles.** To confirm that the  
404 introduction of the reporter construct into the *Dbp* locus did not alter circadian clock function, molecular



405 and behavioral rhythms were assessed. Mice used for these analyses had either one or two copies of the  
406 GFP-containing conditional allele ( $Dbp^{KI/+}$  and  $Dbp^{KI/KI}$ , respectively), one or two copies of the luciferase-  
407 expressing allele ( $Dbp^{Luc/+}$  and  $Dbp^{Luc/Luc}$ , respectively), or were wild-type (WT) littermate controls.

408 RNA was isolated from male livers collected at 4-h intervals over 24-h in a 12L:12D (LD)  
409 lighting cycle. Northern blots were prepared and probed for *Dbp* and *Actin* (loading control). As expected,  
410 the transcripts from  $Dbp^{KI}$  and  $Dbp^{Luc}$  alleles migrated more slowly than the wild-type transcript (**Fig.**  
411 **2A**), due to inclusion of GFP and luciferase coding sequence in these transcripts, respectively, as verified  
412 by probing for reporter sequences in a separate blot. Peak levels of *Dbp* expression in liver occurred at  
413 ZT10 in all genotypes (**Fig. 2B, 2C**), as expected based on previous studies<sup>3,42,57</sup>. For each transcript type,  
414 the *Dbp/Actin* ratios were ranked within each series of 6 timepoints. These ranks differed significantly  
415 among the timepoints for each transcript (Friedman's One-Way analysis of variance,  $p < 0.002$ ), and post-  
416 hoc testing indicated significantly higher rankings at ZT10 than at ZT2, ZT18 and ZT22 (Dunn's test,  $p <$   
417  $0.05$ ; Fig 2D-2F). These data indicate that the temporal profile of transcript expression from the *Dbp*  
418 locus was unaffected by the inclusion of reporter sequences.

419 Heterozygous mice expressed both *Dbp* and *Dbp-plus-reporter* transcripts. The two transcript  
420 types did not differ in abundance: optical density over film background of the  $Dbp^{KI}$  transcript was  $100.5$   
421  $\pm 5.3$  % of the  $Dbp^+$  transcript in  $Dbp^{KI/+}$  mice ( $t=0.084$ ,  $df=7$ ,  $p=0.94$ , one-sample t-test vs 100%), while  
422 the  $Dbp^{Luc}$  transcript was  $102.3 \pm 5.0$  % of  $Dbp^+$  transcript in  $Dbp^{Luc/+}$  mice ( $t=0.446$ ,  $df=7$ ,  $p=0.669$ ). The  
423 equivalent expression level of the two transcript types in heterozygous animals strongly suggests that  
424 transcript regulation and stability were not altered by inclusion of reporter-encoding sequences.

425 Locomotor activity rhythms were assessed in constant darkness in mice of both sexes in the same  
426 five genotypes (**Table 1; Fig. S1**). We found a significant sex-by-genotype interaction ( $F_{4,102} = 2.904$ ,  $p =$   
427  $0.0254$ ). Post-hoc tests indicated an unexpected sex difference in the  $Dbp^{Luc/Luc}$  mice. Indeed, when this  
428 genotype was excluded from the analysis, no significant sex-by-genotype interaction was observed ( $F_{3,88}$   
429  $= 1.349$ ;  $p = 0.2636$ ) and one-way ANOVA did not find a significant main effect of genotype ( $F_{3,91} =$   
430  $1.174$ ;  $p = 0.3242$ ). One-way ANOVA within each sex with all five genotypes included revealed no

431 genotype effect in males ( $F_{4,50} = 1.299$ ,  $p = 0.283$ ). While there was a significant genotype effect in  
432 females ( $F_{4,52} = 2.716$ ,  $p = 0.040$ ), Tukey HSD post-hoc tests did not find a significant result among any  
433 of the pairwise genotype comparisons (all  $p$  values  $> 0.05$ ). Similarly, an alternative post-hoc analysis  
434 revealed that none of the other female genotypes differed from WT females in their free-running period in  
435 constant darkness (Dunnett's test,  $p > 0.5$  in each case). To further examine the effect of sex on free-  
436 running period, males and females of each genotype were compared directly. In both  $Dbp^{Luc/Luc}$  and  
437  $Dbp^{KI/KI}$  mice, males had significantly longer periods than females ( $p < 0.01$ ), while there was no sex  
438 difference in wild-types or heterozygous reporters ( $p > 0.46$ ).

439 Together, these assessments of molecular and behavioral rhythms indicate that the reporter alleles  
440 do not change  $Dbp$  expression or appreciably alter circadian function.

441  
442 **GFP expression from the  $Dbp^{KI}$  allele.** To examine expression of GFP from the conditional allele,  
443  $Dbp^{KI/+}$  mice (n=5-6 mice per time-point) were anesthetized and perfused with fixative at 4-h intervals  
444 over 24 h (**Fig. S2**). Liver sections from  $Dbp^{KI/+}$  and control (WT) mice were examined by confocal  
445 microscopy. Fluorescence signal intensity did not differ between time-points (ANOVA  $F_{5,26} = 1.279$ ,  $p =$   
446  $0.7560$ ). GFP signal from  $Dbp^{KI/+}$  liver sections was 5-10x higher than from WT sections, but absolute  
447 levels were quite low. The low level of GFP expression may be due to the use of destabilized GFP with a  
448 2-hour half-life, intended to more accurately track changes on a circadian time-scale. The relatively low  
449 level and lack of detectable rhythmicity in GFP expression was unexpected, especially considering that  
450 liver is the tissue with the highest levels of  $Dbp$  expression (Fonjallaz et al., 1996) and thus may represent  
451 a 'best-case' scenario. As the primary objective of this project was to generate a mouse model with *Cre*-  
452 dependent expression of bioluminescence from the  $Dbp$  locus, however, the absence of robust GFP-  
453 driven fluorescence rhythms in *Cre*-negative cells did not preclude achieving this objective. GFP is  
454 effectively serving as a 'floxed stop' to make luciferase expression from the  $Dbp$  locus exclusively *Cre*-  
455 dependent.

456

457 **Non-conditional luciferase expression from the *Dbp<sup>Luc</sup>* allele.** The *Dbp<sup>Luc</sup>* allele produces widespread,  
458 rhythmic luciferase expression, both *in vivo* and *ex vivo*. More specifically, explants of lung and anterior  
459 pituitary gland from *Dbp<sup>Luc/+</sup>* mice incubated with D-luciferin had robust circadian rhythms in  
460 bioluminescence (**Fig. 3**). Furthermore, *in vivo* imaging of *Dbp<sup>Luc/+</sup>* mice at 7 time-points over a ~30-h  
461 period revealed rhythmic bioluminescence in the abdomen and throat in ventral views, and in the lower  
462 back in dorsal views (**Fig. 4B**), similar to the distribution of bioluminescence signal from *Per2<sup>Luciferase/+</sup>*  
463 (Tahara et al., 2012) and *Per2<sup>LucSV/+</sup>* mice (van der Vinne et al., 2018; van der Vinne et al., 2020) (**Fig.**  
464 **4A**). The level of light output was ~2.5-fold greater in ventral views than in dorsal views ( $p < 0.0001$ ,  
465 Wilcoxon matched pairs test,  $W=151$ ,  $n=17$ ). In the abdomen, a rostral (“liver”) region of interest (ROI)  
466 accounted for  $46.6 \pm 3.0\%$  (Mean  $\pm$  SEM;  $n=17$ ) of bioluminescence from the ventral view, while the  
467 lower abdomen contributed another  $38.4 \pm 3.5\%$ . Bioluminescence rhythms from the throat region of  
468 *Per2<sup>Luciferase</sup>* mice have previously been shown to originate in the submandibular gland (Tahara et al.,  
469 2012). Bioluminescence was absent in mice with wild-type *Dbp* alleles or with the conditional *Dbp<sup>KI</sup>*  
470 allele (in the absence of *Cre*).

471 Previous reports have shown that in a number of tissues, *Dbp* RNA levels peak earlier than *Per2*  
472 RNA levels (Punia et al., 2012; Zhang et al., 2014). Consistent with this literature, the time of peak of  
473 bioluminescence rhythms from *Dbp<sup>Luc/+</sup>* tissues preceded the time of peak of bioluminescence rhythms  
474 from *Per2<sup>LucSV/+</sup>* tissues by ~6 hours in explants (**Fig. 3C, 3F**) and by ~9 hr *in vivo* (**Fig. 4G-4I**).  
475 Bioluminescence rhythms from *Per2<sup>LucSV/+</sup>* tissue explants had significantly longer period than explants  
476 from *Dbp<sup>Luc/+</sup>* mice (Lung:  $25.29 \pm 0.13$  vs  $23.93 \pm 0.11$  h;  $F_{1,27.7} = 95.55$ ,  $p < 0.0001$ ; Anterior Pituitary:  
477  $25.27 \pm 0.08$  vs  $23.73 \pm 0.112$  h;  $F_{1,24.53} = 66.12$ ,  $p < 0.0001$ ).

478  
479 **Cre-dependent Luciferase Expression in Liver.** The main use we envision for the *Dbp* reporter alleles  
480 involve *Cre* recombinase-mediated excision of GFP, leading to expression of *luciferase* in cells  
481 expressing *Cre*. The effectiveness of this approach was first assessed in hepatocytes using an *Albumin-*  
482 *Cre*-driver line. *In vivo* bioluminescence imaging of intact *Albumin-Cre<sup>+</sup>*; *Dbp<sup>KI/+</sup>* “liver reporter” mice at

483 the time of expected maximal bioluminescence revealed that  $96.6 \pm 0.48\%$  of light originated in the  
484 “liver” ROI (relative to total ventral-view bioluminescence;  $p < 0.0001$  versus  $46.6 \pm 3.0\%$  in *Dbp<sup>Luc</sup>* mice,  
485 U-test,  $U=0$ ,  $n=19$  and  $17$ , respectively). Notably, post-mortem imaging after dissection confirmed that  
486 bioluminescence originated exclusively from the liver in these mice ( $97.4\%$  of light from liver;  $n=12$ ).

487 In a separate cohort of liver reporter mice, bioluminescence was assessed around the clock by  
488 IVIS imaging. The cosinor-fitted time of peak of *Dbp*-driven bioluminescence rhythms from the liver  
489 ‘region of interest’ of these mice (ZT11) was indistinguishable from the peak time of the liver ROI  
490 analyzed in whole-body *Dbp<sup>Luc</sup>* mice (**Fig. 4I**).

491  
492 **Cre-dependent Luciferase Expression in Kidney.** Viral introduction of rhythmic luciferase reporters to  
493 the liver has been used previously (Saini et al., 2013, Sinturel et al., 2021), so our success with detecting  
494 bioluminescence rhythms specifically from the liver in *Albumin-Cre<sup>+</sup>*; *Dbp<sup>KI/+</sup>* “liver reporter” mice was  
495 reassuring, but not surprising. With reporter genes expressing from multiple tissues (e.g., *Dbp<sup>Luc</sup>* and  
496 *Per2<sup>Luc</sup>*), the contribution made by surrounding organs may be unclear. To extend our demonstration of  
497 tissue-specific luciferase expression from the conditional *Dbp<sup>KI</sup>* allele, we examined bioluminescence  
498 from anesthetized *Ksp1.3-Cre*; *Dbp<sup>KI/+</sup>* “kidney reporter” mice. The *Ksp1.3-Cre* driver leads to  
499 recombination in the developing kidney and urogenital tissues, and in renal tubules of adult mice. In male  
500 kidney reporter mice, IVIS imaging of anesthetized, dissected living mice revealed bioluminescence from  
501 the kidney and seminal vesicles *in situ* (**Fig. S3, S4**). In females, bioluminescence originated from the  
502 kidney and proximal ureter (**Fig. S5**). We thus used female mice to assess rhythmicity. Clear diurnal  
503 rhythmicity in bioluminescence was apparent from the kidney (Friedman’s One-Way Analysis of  
504 Variance, ( $F_r = 32.71$ ,  $k=5$ ,  $n=9$ ,  $p < 0.0001$ , see **Fig. S6**), with a peak at ZT8. Dunn’s test revealed that ZT8  
505 timepoint differed significantly from ZT0 and ZT18 but not from ZT4 and ZT14 (multiplicity-corrected,  
506 two-tailed Dunn’s test; see **Fig. S6**).

507

508 **Cell-type Specific Bioluminescence Rhythms in SCN Slices.** The heterogeneity of SCN neurons has  
509 important functional implications for our understanding of the central circadian clock (Herzog et al.,  
510 2017). Neuromedin S (NMS) is expressed in ~40% of SCN cells, while Arginine Vasopressin (AVP) is  
511 expressed in ~10% of SCN neurons and is contained within the NMS-expressing population (Lee et al.,  
512 2015). The utility of our conditional reporter line was demonstrated by monitoring bioluminescence  
513 rhythms within specific subpopulations of SCN neurons (**Fig. 5**). *NMS-iCre; Dbp<sup>KI/+</sup>* mice and *AVP-*  
514 *IRES2-Cre; Dbp<sup>KI/+</sup>* mice were generated, and single-cell bioluminescence rhythms were compared to  
515 those from non-conditional *Dbp<sup>Luc/+</sup>* mice in SCN slices *ex vivo*. For the conditional mice,  
516 bioluminescence was apparent in subsets of cells within the SCN (**Fig. 5A**). The anatomical pattern of  
517 bioluminescence in the SCN differed based on the *Cre* line used, consistent with the expected distribution  
518 for each neuronal subtype.

519 The cell-type specificity of bioluminescence signals from the different genotypes enabled the  
520 assessment of rhythm quality in the different neural populations. This assessment revealed a significantly  
521 shorter period in AVP<sup>+</sup> cells compared to NMS<sup>+</sup> cells (**Fig. 5D**;  $F_{2,14.64} = 4.259$ ,  $p = 0.0345$ ). Although the  
522 time of peak of *Dbp*-driven bioluminescence did not differ significantly between the different cellular  
523 populations examined (**Fig. 5E**;  $F_{2,18.31} = 0.6570$ ,  $p = 0.5302$ ), a reduction in rhythm robustness was  
524 observed in AVP<sup>+</sup> neurons compared to rhythms of NMS<sup>+</sup> neurons as well as compared to all cells (**Fig.**  
525 **5F**;  $F_{2,18.11} = 14.34$ ,  $p = 0.0002$ ). The distribution of peak times was also more dispersed in AVP<sup>+</sup> cells  
526 compared to NMS<sup>+</sup> cells (**Fig. 5G**).

527 These results complement the recent report from Shan *et al.* (2020) using a *Cre*-dependent Color-  
528 Switch PER2::LUC reporter mouse demonstrating period and phase differences among sub-populations  
529 of SCN neurons. Our *Dbp<sup>KI</sup>* mice and the recently reported Color-Switch PER2::LUC mouse line (Shan *et*  
530 *al.*, 2020) will be important additions to our molecular-genetic armamentarium for unravelling the  
531 complicated relationships among the cellular components of the SCN circadian pacemaker<sup>58-64</sup>.

532

533 **Continuous, Non-invasive Detection of Bioluminescence Rhythms from Liver in Ambulatory Mice.**

534 Addressing issues of internal desynchrony and misalignment of oscillators requires monitoring the  
535 dynamics of tissue resetting over time after a phase-shifting stimulus. The use of *in vivo* bioluminescence  
536 imaging for repeated assessments of organ-level regions of interest over multiple days is feasible but  
537 requires several potentially disruptive anaesthesia sessions (Poulsen et al., 2018) per circadian cycle. As a  
538 result, *in vivo* bioluminescence imaging has generally been relegated to assessing phase of reporter gene  
539 oscillations on relatively few occasions after a shifting stimulus, with rare exception (van der Vinne et al.,  
540 2020). Other methods for monitoring bioluminescence and fluorescence rhythms in ambulatory mice have  
541 been developed (Hamada et al., 2016; Mei et al., 2018; Nakamura et al., 2008; Ono et al., 2015; Saini et  
542 al., 2013; Sawai et al., 2019; Yamaguchi et al., 2016; Yamaguchi et al., 2001), but a less invasive  
543 approach for assessing rhythms in a variety of specific tissues is desirable. In addition, several abdominal  
544 organs emit significant amounts of bioluminescence in “whole-body” reporter mice, including liver,  
545 kidney and intestines. These tissues likely overshadow (or, more accurately, out-glow) surrounding  
546 tissues. Bioluminescence from even larger organs like liver and kidney is likely ‘contaminated’ by light  
547 from adjacent structures.

548 To overcome these difficulties with assessing the origin of bioluminescence in “whole-body”  
549 reporter mice, and to refine recently developed methods for long-term monitoring of peripheral rhythms  
550 in ambulatory mice (Martin-Burgos et al., 2020), we performed studies using *Albumin-Cre; Dbp<sup>KI/+</sup>*  
551 (“liver reporter”) mice. First, we examined the potential impact of route of substrate administration on  
552 rhythm phase using the Lumicycle *In Vivo* system (Actimetrics, Wilmette IL). Mice were entrained to LD  
553 followed by a skeleton photoperiod consisting of four 1-h pulses of light every 24 hr  
554 (1L:1D:1L:6D:1L:1D:1L:12D) with the 12-h dark phase coinciding with 12-h dark phase of the  
555 preceding LD cycle. A skeleton photoperiod was used because detection of bioluminescence requires the  
556 absence of ambient light, while studies of light-induced phase shifting obviously require light; a skeleton  
557 photoperiod is a compromise between these conflicting constraints. After 7 days in the skeleton  
558 photoperiod, mice were anesthetized for subcutaneous implantation of a primed osmotic minipump

559 (Alzet, Model #1002 (0.25 $\mu$ l per hour)) containing either D-luciferin (100 mM) or phosphate buffered  
560 saline (PBS). Mice with PBS-containing pumps received D-luciferin in the drinking water (2 mM). The  
561 time of peak bioluminescence was determined by discrete wavelet transform (DWT) analysis on the first  
562 day of exposure to constant darkness (5 days after pump implantation). There was no difference in time of  
563 peak between these routes of administration (drinking water: mean peak time ( $\pm$  SEM) CT  $8.75 \pm 0.20$  (n  
564 = 7); osmotic minipumps: mean peak time CT  $8.76 \pm 0.19$  (n=7); unpaired t-test,  $t = 0.0342$ ,  $df = 12$ ,  $p =$   
565  $0.9733$ ). Thus, the presumed rhythm of substrate intake, secondary to the rhythm of water intake, does not  
566 change the time of peak of the bioluminescence rhythm. This is consistent with recent results from  
567 Sinturel et al., (2021). Subsequent studies used D-luciferin (2 mM) administered in the drinking water.

568

569 **Circadian Misalignment Following a Phase Shift of the Lighting Cycle.** The approach described  
570 above provides an unparalleled system for assessing the timing of rhythmicity in a specific tissue over  
571 long periods of time. Next, hepatic bioluminescence rhythms were monitored in *Albumin-Cre; Dbp<sup>KI/+</sup>*  
572 (liver reporter) mice before and after a 6-hr phase advance of the skeleton lighting cycle. Mice that  
573 remained in the original (non-shifted) skeleton lighting regimen had a stable phase of hepatic  
574 bioluminescence (**Fig. 6C**). In contrast, mice exposed to a phase-advance of the skeleton photoperiod  
575 displayed a gradual phase-advance in both locomotor activity and hepatic bioluminescence rhythms (**Fig.**  
576 **6A, B**). Notably, locomotor rhythms shifted more rapidly than hepatic bioluminescence (**Fig. 6B**). To  
577 compare the re-entrainment of bioluminescence and locomotor activity rhythms, peak time for each  
578 rhythm each day was normalized to the time of peak on the last day before shifting the lighting cycle in  
579 the shifted group (e.g., Day 2 in **Fig. 6**) for each animal. Data from each lighting group were analyzed  
580 separately using a general linear model with Animal ID as a random variable (allowing comparison of the  
581 two rhythms within individuals) and the main effects were endpoint (locomotor activity or  
582 bioluminescence) and Day number. In animals not undergoing a phase shift, the phase relationship of  
583 these endpoints was unchanged over time ( $F < 1.1$ ,  $p > 0.39$ ). In contrast, in animals exposed to a 6-hr  
584 phase advance, the phase relationship of the locomotor activity and bioluminescence rhythms differed

585 significantly (Measure\*Day interaction,  $F_{9,54.98} = 3.358$ ,  $p = 0.0024$ ). Post-hoc testing revealed a  
586 significant difference in phase between the two measures on day 9 (Tukey HSD,  $p < 0.05$ ). A separate  
587 analysis to compare phase (relative to Day 2 baseline) between bioluminescence and locomotor activity  
588 rhythms revealed significant differences between the two measures on days 5, 6, 7, 8, 9 and 10 (t-tests on  
589 each day,  $p < 0.05$ ). Thus, both locomotor activity and hepatic bioluminescence rhythms shifted following  
590 a phase shift of the lighting cycle, but the rhythms differ in their kinetics of re-adjustment: liver lagged  
591 behind. These data provide clear evidence for misalignment of SCN-driven behavioral rhythms and  
592 hepatic rhythmicity.

593

594 **Recovery from Circadian Misalignment Induced by Temporally Restricted Feeding.** We next  
595 conducted a study to examine misalignment induced by restricted feeding. Previous studies have shown  
596 that food availability limited to daytime significantly alters phase of peripheral oscillators (Damiola et al.,  
597 2000; Hara et al., 2001; Stokkan et al., 2001; Saini et al., 2013). Due to our desire to study  
598 bioluminescence rhythms without interference from the LD cycle, we administered different feeding  
599 regimens in an LD cycle and then assessed the hepatic bioluminescence rhythm after release to DD with  
600 *ad libitum* food. This allowed us to determine the time of peak bioluminescence of the liver after  
601 restricted feeding, and the opportunity to continuously observe its return toward a normal phase  
602 relationship with SCN-driven behavioral rhythms over time.

603 *Alb-Cre;Dbp<sup>KI/+</sup>* liver reporter mice were exposed to one of three feeding regimes (*ad libitum*,  
604 nighttime, or daytime food availability; **Fig. 7A**) for ten days in LD before recording bioluminescence in  
605 DD with *ad libitum* food availability. A previously described automated feeder system (Acosta-Rodriguez  
606 et al., 2017) was used to restrict food availability. This system limits total daily consumption (to prevent  
607 hoarding) and restricted food pellet delivery for day-fed mice to 0600-1800 h (ZT0-ZT12), and for night-  
608 fed mice to 1800-0600 h (ZT12 – ZT24/0). With the setting used, the system restored daily food  
609 allotments to *ad libitum* fed and night-fed mice daily at 0000h (ZT18), resulting in unusual temporal  
610 profiles of food intake in *ad libitum* and night-fed mice. Nevertheless, *ad libitum* and nighttime food



611 access both resulted in food intake being concentrated in the night, while daytime food availability  
612 resulted in the midpoint of food intake occurring during the first half of the light phase (**Fig. 7A, 7B, 7C**).  
613 Within-group variability in the timing of food intake was low except for three clear outliers (**Fig. 7C**) that  
614 were excluded from subsequent analyses.

615 *Ad libitum* fed mice showed consistently phased rhythms in bioluminescence after transfer to DD  
616 from LD, as did night-fed animals (**Fig. 7A, 7D**). In contrast, mice fed only during the light period for 10  
617 days prior to housing in DD with *ad libitum* food had an earlier peak time of the hepatic bioluminescence  
618 rhythm. Daytime feeding resulted in a significantly advanced peak time compared to both night-fed and  
619 *ad libitum* fed mice, while these latter groups were statistically indistinguishable ( $F_{2,259.6} = 76.66, p <$   
620  $0.0001$ ; **Fig. 7D**). Subsequent exposure to DD with *ad libitum* feeding allowed the hepatic clock of day-  
621 fed mice to return toward the appropriate phase relationship with the locomotor activity rhythm.

622 Although daytime feeding resulted in an advanced time of peak bioluminescence, the timing of  
623 the liver bioluminescence rhythm was not solely controlled by the timing of food intake. First, no  
624 significant correlations between the timing of food intake and time of peak bioluminescence were  
625 observed within any of the three feeding regimes ( $F < 1.13, p > 0.32$ ; **Fig. 7C**). Second, the relationship  
626 between the timing of liver bioluminescence rhythms relative to the midpoint of food intake was  
627 significantly different between the different groups ( $F_{2,17} = 313.2, p < 0.0001$ ; **Fig. 7E**). While *Dbp*-driven  
628 hepatic bioluminescence rhythms were roughly in anti-phase with the midpoint of feeding in *ad libitum*  
629 and night-fed mice, daytime feeding resulted in near synchrony between these rhythms (**Fig. 7E**).  
630 Furthermore, although the average midpoint of feeding was significantly earlier in night-fed compared to  
631 *ad libitum* fed mice ( $t_{10} = 6.21, p < 0.0001$ ; **Fig. 7C**), no significant difference was observed in  
632 bioluminescence phase relative to the preceding light-dark cycle (**Fig. 7D**), with the timing of liver  
633 bioluminescence rhythms relative to the midpoint of food intake being significantly delayed in night-fed  
634 compared to *ad libitum* fed mice (**Fig. 7E**). Overall, these results demonstrate that although the timing of  
635 food intake strongly influences liver rhythms, the timing of bioluminescence rhythmicity in liver reporter

636 mice is not solely driven by the timing of food intake (with food intake regulated for this duration and in  
637 this way).

638

## 639 **Discussion**

640 Numerous studies have made use of rhythmically expressed bioluminescent reporter genes to  
641 monitor circadian rhythms. The *Per2<sup>Luciferase</sup>* mouse and other reporters with bioluminescence under the  
642 control of a clock gene have been especially useful as they generate robust bioluminescence rhythms from  
643 numerous tissues recorded *ex vivo* (Abe et al., 2002; Maywood et al., 2013; Yakazami et al., 2000;  
644 Yamazaki and Takahashi, 2005; Yoo et al 2004; Yoo et al., 2005). The widespread expression of  
645 PER2::LUCIFERASE (and other ‘non-conditional’ bioluminescence reporters) comes at a cost, however,  
646 as it is not possible to assess rhythmicity in specific cell populations within a larger tissue without  
647 dissection. Tissue explant preparation can cause phase-resetting, however, especially after exposure to  
648 phase shifting stimuli (Noguchi et al., 2020; Leise et al., 2020). Furthermore, *ex vivo* culturing of tissues  
649 does not allow assessment of rhythmicity in the context of the hierarchical circadian system or dynamic  
650 changes during environmentally-induced resetting.

651 We chose to modify the *Dbp* gene to generate a conditional reporter for several reasons. *Dbp* is  
652 widely and rhythmically expressed at readily detectable levels (Fonjallaz et al., 1996; Punia et al., 2012;  
653 Zhang et al., 2014). This feature ensures that the reporter mouse would be useful for detecting rhythmicity  
654 in numerous tissues. In addition, individual clock genes are responsive to different signaling pathways.  
655 This differential regulation can lead to circadian misalignment *within* the circadian clock (Reddy et al.,  
656 2002; Nicholls et al., 2019). As an output gene controlled by the CLOCK:BMAL1 transcriptional  
657 activator complex (Ripperger & Schibler 2006; Stratmann et al., 2012), *Dbp* rhythmicity is likely a good  
658 proxy for the integrated output of the molecular clockwork. Finally, concern that the targeting event could  
659 disrupt function of the modified gene led us to steer away from core clock genes. Mice homozygous for a  
660 targeted allele of *Dbp* have only a modest circadian phenotype (Lopez-Molina et al., 1997).  
661 Homozygotes of both the *Per2<sup>LucSV</sup>* and *Per2<sup>Luciferase</sup>* lines have altered circadian rhythms (Ralph et al.,

662 2020; Yoo et al., 2017; see below). The GFP-expressing *Dbp* transcript lacks the native 3' UTR and uses  
663 an exogenous polyadenylation sequence, which could affect *Dbp* gene expression and regulation.  
664 Notably, however, our Northern blot analysis suggests little or no alteration in expression level or  
665 dynamics of the *Dbp* reporter transcripts.

666 Yoo et al. (2017) reported that homozygous *Per2*<sup>LucSV/LucSV</sup> mice (in which a SV40  
667 polyadenylation site is used instead of the endogenous *Per2* 3' UTR) have a longer period length of  
668 locomotor activity rhythms in DD and explant bioluminescence rhythms *ex vivo* than the more widely  
669 used *Per2*<sup>Luciferase</sup> reporter. The potential impact of a single *Per2*<sup>LucSV</sup> allele (as used in our studies) on  
670 period length has not been reported, but this could contribute to the longer period of *Per2*<sup>LucSV/+</sup> explants,  
671 relative to *Dbp*<sup>Luc/+</sup> explants. Interestingly, Ralph et al., (2020) recently reported that the *Per2*<sup>Luciferase</sup>  
672 reporter that uses the endogenous *Per2* 3'UTR (Yoo et al., 2004) also has longer period in DD and other  
673 circadian phenotypes. Tosini and colleagues have also recently reported retinal degeneration and  
674 alterations in classical photoreception in aged male *Per2*<sup>Luciferase/Luciferase</sup> mice (Goyal et al., 2021).

675 Shan et al. (2020) recently reported development of a Color-Switch PER2::LUC line which was  
676 used to demonstrate the utility of a Cre-dependent reporter approach for interrogating SCN circuitry. The  
677 Color-Switch PER2::Luc line has the advantage of reporting on both Cre-positive and Cre-negative cells  
678 in different colors. Detection of bioluminescence from the Color-Switch PER2::LUC reporter requires  
679 segmentation of the bioluminescence signal between wavelengths. Our 'simpler' approach of only  
680 inducing a bioluminescence signal in *Cre*-positive cells of *Dbp*<sup>KI/+</sup> mice enables recording of  
681 bioluminescence rhythms without the need for wavelength segmentation. In addition, the *Dbp* reporter  
682 can easily be used in *Per2* mutant mice. Like the Color-Switch PER2::LUC line, our *Dbp* conditional  
683 reporter line is useful for *ex vivo* studies, allowing specific cellular populations to be monitored by  
684 crossing to the appropriate *Cre*-expressing lines.

685 Our studies reveal subtle differences among the population of oscillators defined by *AVP-Cre*,  
686 *NMS-Cre*, and the entire SCN cohort. More specifically, *AVP* cells had a shorter period, reduced

687 rhythmicity index, and larger within-slice dispersal of peak times than the NMS cell population with  
688 which it overlaps. Our results suggest that AVP cells are coordinated less well and are less robust than  
689 other populations in the SCN. This suggestion is in contrast to the typical view of AVP cells as high-  
690 amplitude ‘output’ neurons that also contribute to determination of period and rhythm amplitude (Herzog  
691 et al., 2017; Mieda et al., 2015; Mieda et al., 2016). One possible explanation for this is that AVP may be  
692 dysregulated in the AVP-Cre line (Cheng et al., 2019), influencing function of the SCN as a whole in the  
693 *AVP-IRES-Cre; Dbp<sup>KI/+</sup>* genotype. Of note for circadian researchers, both the AVP-IRES-Cre and a VIP-  
694 IRES-Cre line influence neuropeptide expression and circadian function (Cheng et al., 2019; Joye et al.,  
695 2020).

696 We envision this line will be very useful for monitoring additional neuronal subpopulations in the  
697 SCN in wild-type and mutant animals. Additional technical development may allow *in vivo* detection of  
698 bioluminescence rhythms from neuronal populations in awake behaving mice. Approaches to optimize  
699 the signal detected from brain include use of highly efficient and cell- and brain-penetrant substrates  
700 (Evans et al., 2014; Iwano et al., 2018), cranial windows (Miller et al., 2014) and hairless or albino mice  
701 (Martin-Burgos et al., 2020; Iwano et al., 2018). (Note, the tyrosinase mutation leading to albinism in  
702 C57BL/6J mice is linked to *Dbp* on mouse chromosome 7; we have nevertheless generated recombinants  
703 and produced albino reporters, including the kidney reporter mice in Fig. **S2**). These approaches may  
704 allow interrogation of the SCN circuit *in vivo*, extending the elegant studies being performed with SCN  
705 slices *ex vivo*. Bioluminescence rhythms can also be examined in neuronal populations outside the SCN,  
706 by using an appropriate *Cre* driver and/or viral delivery of *Cre* recombinase.

707 *In vivo* bioluminescent imaging allows assessment of bioluminescence from several organs *in*  
708 *vivo*, but the signal from these areas likely includes light emitted from nearby organs (e.g., intestinal tract  
709 and abdominal fat likely contribute to the signal attributed to liver and kidney). Indeed, the size and shape  
710 of the “liver” ROI seen by IVIS imaging differs between *Dbp* liver reporter mice and whole-body reporter  
711 *Dbp<sup>Luc</sup>* mice. Furthermore, bioluminescence from nearby tissues can be obscured by the high level of light  
712 coming from liver, kidney and intestines. *Cre*-mediated recombination of the conditional *Dbp* reporter

713 allele thus enables assessment of bioluminescence from kidney and liver, separately, and also from other  
714 tissues.

715 *Cre*-mediated recombination of the *Dbp<sup>KI</sup>* allele in liver enabled us to perform continuous, *in vivo*  
716 bioluminescence monitoring of liver in freely moving mice. These studies demonstrate transient  
717 misalignment between the liver oscillator and SCN-regulated behavioral rhythms. Our design is  
718 complementary to that used by Saini et al. (2013), who continuously monitored reporter gene  
719 bioluminescence as hepatic rhythms were shifted by an inverted feeding regimen.

720 Repeated misalignment among oscillators is thought to contribute to adverse metabolic and health  
721 consequences of chronic circadian disruption (for reviews, see Arble et al., 2015; Evans and Davidson,  
722 2013; Roenneberg and Mellow, 2016; Patke et al., 2020; West & Bechtold, 2015). Up until now,  
723 technical and practical limitations have restricted our ability to monitor the behavior of circadian rhythms  
724 in different peripheral tissues during and following environmental disruption of circadian homeostasis.  
725 Our *Cre*-conditional reporter line and the approaches described recently by Martin-Burgos et al. (2020)  
726 and extended here for longitudinal and tissue-specific assessment of bioluminescence rhythms *in vivo* will  
727 allow characterization of misalignment and recovery after a variety of circadian-disruptive lighting and  
728 food availability paradigms. These approaches will allow more extensive examination of the  
729 consequences of repeated misalignment of peripheral clocks.

730 Previous studies have shown misalignment between central and peripheral clocks induced by  
731 altering the time of food access to daytime, by assessing oscillator phase at various time-points after a  
732 phase shift of the lighting cycle, or by exposure to non-24hr light-dark schedules. The vast majority of  
733 these studies monitored bioluminescence rhythms *ex vivo* or assessed transcript levels following tissue  
734 collection at various times after a shift (Balsalobre et al., 2000; Damiola et al., 2000; Davidson et al.,  
735 2008; Davidson et al., 2009; Nakamura et al., 2005; Nicholls et al., 2019; Pezuk et al., 2012; Sellix et al.,  
736 2012; Stokkan et al., 2001; Yamanaka et al., 2008). Notably, *ex vivo* bioluminescence rhythm timing may  
737 be affected by prior lighting conditions (Noguchi et al., 2020; Leise et al., 2020; Tahara et al., 2012). Few  
738 studies have followed bioluminescence rhythms *in vivo* over time after a light-induced phase shift or after

739 a food manipulation that phase-shifts peripheral oscillators (but see Saini et al., 2013; van der Vinne et al.,  
740 2020). Our current data leverage the ability to non-invasively monitor rhythmicity from a single  
741 peripheral oscillator in individual animals over many days to show the time course of internal  
742 misalignment and recovery after a phase shift. Other studies with minimally invasive monitoring of  
743 bioluminescence rhythms have relied upon viral introduction of the reporter into liver, and thus cannot  
744 easily be extended to other tissues (Saini et al., 2013; Sinturel et al., 2021). Notably, the viral reporter  
745 appears not strictly limited to liver in this model (see Saini et al. 2013, their Fig S2). Moreover, efficient  
746 expression of virally delivered reporter constructs is limited by the promoter size and specificity, so the  
747 level and anatomical pattern of expression often do not match that of the gene whose promoter was used.  
748 Future studies of additional tissues in *Cre*-conditional reporter mice will enable elucidation of how other  
749 tissues within the hierarchical, multi-oscillatory circadian system respond to disruptive stimuli. Several  
750 studies suggest that organs differ in their response to resetting stimuli. For example, the *Dbp* mRNA  
751 rhythm in liver is more fully reset than the rhythm in heart and kidneys 3 days after restricting food  
752 availability to daytime (Damiola et al., 2000), and several studies indicate the SCN (and the locomotor  
753 rhythms it regulates) resets more rapidly than peripheral tissues (Davidson et al., 2008; Davidson et al.,  
754 2009; Damiola et al., 2000; Hamada et al., 2016; Saini et al., 2013; Sellix et al., 2012; van der Vinne et  
755 al., 2020; Yamanaka et al., 2008; Yamazaki et al., 2000; see Nicholls et al., 2019 for review).

756 A further advance in studying the behavior of peripheral oscillators is provided by the ability to  
757 temporally regulate the timing of feeding (Acosta-Rodriguez et al, 2017). A recent study used a feeding  
758 device similar to the one used here to recapitulate ‘naturalistic’ food intake patterns in mice with  
759 restricted food access (Xie et al., 2020), meaning the food restriction was not the severe ‘all or none’  
760 patterns typically used in studies with time-restricted access to food. The authors found that peripheral  
761 oscillators of *Per2<sup>Luciferase</sup>* mice were not effectively entrained by restricted feeding using the imposed  
762 ‘natural’ feeding patterns (Xie et al., 2020). Our restricted food access study produced a smaller and more  
763 variable phase shift of the hepatic circadian clock (as indicated by the initial time-of-peak of *Dbp*-driven  
764 bioluminescence) than expected based on published results using presence / absence food availability

765 cycles (Damiola et al., 2000; Hara et al., 2001; Saini et al., 2013; Stokkan et al., 2001). A longer period of  
766 adjustment to the restricted feeding schedule or more complete and abrupt transitions between food  
767 presence and absence would likely produce a stronger entraining signal for the liver. Future use of a  
768 variety of different *Cre* drivers will allow assessment of whether different peripheral organs respond  
769 similarly to food restriction paradigms. In addition, tissue-specific reporter models will be very useful in  
770 assessing how more naturalistic food ingestion paradigms influence peripheral circadian clocks in several  
771 tissues.

772         In summary, we have demonstrated the utility of a new, Cre-conditional reporter mouse that  
773 enables tissue-specific monitoring of circadian molecular rhythms *in vivo* and *ex vivo*. This reporter  
774 mouse provides a major advance in our capabilities for monitoring rhythms in a variety of tissues under  
775 normal and disruptive conditions, which is a key step in the identification of mechanisms underlying the  
776 adverse consequences of circadian disruption inherent to life in modern 24/7 societies.

777

778 **Acknowledgments**

779 We thank Christopher Lambert and Jamie Black for technical assistance, and Steven A. Brown  
780 (University of Zurich) for discussions during the development of this project. UMass Medical School core  
781 facilities (Mutagenesis Core, Mouse Modeling Core, and Small Animal Imaging Core) are gratefully  
782 acknowledged.

783 Research reported in this publication was supported by the National Institute for Neurological  
784 Diseases and Stroke and the National Institute of General Medical Sciences of the National Institutes of  
785 Health under award numbers R21NS103180 (DRW), SC1GM112567 (AJD), and NIGMS  
786 R15GM126545 (MEH), the Hartmann Müller Stiftung (RD), MRC MC\_PC\_15070 (RD) and BSN (RD  
787 and LAG). CBS was a participant in the UMass Medical School Initiative for Maximizing Student  
788 Development, supported by NIH grant R25GM113686. The funders had no role in study design, data  
789 collection and analysis, decision to publish, or preparation of the manuscript. The content is solely the  
790 responsibility of the authors and does not necessarily represent the official views of the National Institutes  
791 of Health or the other funding agencies.

792

793 **Author Contributions**

794 R.D and D.R.W. conceived the project  
795 C.B.S., V.v.d.V., E.M., M.H.B., A.J.D., M.E.H., R.D. and D.R.W. designed research  
796 C.B.S., V.v.d.V., E.M., A.C.S., B.M.B., P.C.M., L.A.G., R.D., and D.R.W. performed research  
797 C.B.S., V.v.d.V., E.M., T.L.L., B.M.B., M.E.H., R.D. and D.R.W. analyzed data  
798 C.B.S., V.v.d.V., and D.R.W. wrote the paper  
799 All authors have approved this version of the manuscript.

800



801 **References.**

- 802
- 803 Abe M, Herzog ED, Yamazaki S, Straume M, Tei H, Sakaki Y, Menaker M, and Block GD (2002)
- 804 Circadian rhythms in isolated brain regions. *J Neurosci* 22:350-356.
- 805 Acosta-Rodriguez VA, de Groot, M H M, Rijo-Ferreira F, Green CB, and Takahashi JS (2017) Mice
- 806 under caloric restriction self-impose a temporal restriction of food intake as revealed by an automated
- 807 feeder system. *Cell Metab* 26:267-277.e2.
- 808 Balsalobre A, Brown SA, Marcacci L, Tronche F, Kellendonk C, Reichardt HM, Schutz G, and Schibler
- 809 U (2000) Resetting of circadian time in peripheral tissues by glucocorticoid signaling. *Science*
- 810 289:2344-2347.
- 811 Brandes C, Plautz JD, Stanewsky R, Jamison CF, Straume M, Wood KV, Kay SA, and Hall JC (1996)
- 812 Novel features of *Drosophila period* transcription revealed by real-time luciferase reporting. *Neuron*
- 813 16:687-692.
- 814 Cesbron F, Brunner M, and Diernfellner AC (2013) Light-dependent and circadian transcription dynamics
- 815 *in vivo* recorded with a destabilized luciferase reporter in *Neurospora*. *PLoS One* 8:e83660.
- 816 Chen Z, Yoo SH, Park YS, Kim KH, Wei S, Buhr E, Ye ZY, Pan HL, and Takahashi JS (2012)
- 817 Identification of diverse modulators of central and peripheral circadian clocks by high-throughput
- 818 chemical screening. *Proc Natl Acad Sci U S A* 109:101-106.
- 819 Cheng AH, Fung SW, and Cheng HM (2019) Limitations of the AVP-IRES2-Cre (JAX #023530) and
- 820 VIP-IRES-Cre (JAX #010908) models for chronobiological investigations. *J Biol Rhythms* 34:634-
- 821 644.
- 822 Damiola F, Le Minh N, Preitner N, Kornmann B, Fleury-Olela F, and Schibler U (2000) Restricted
- 823 feeding uncouples circadian oscillators in peripheral tissues from the central pacemaker in the
- 824 suprachiasmatic nucleus. *Genes Dev* 14:2950-2961.
- 825 Davidson AJ, Castanon-Cervantes O, Leise TL, Molyneux PC, and Harrington ME (2009) Visualizing jet
- 826 lag in the mouse suprachiasmatic nucleus and peripheral circadian timing system. *Eur J Neurosci*
- 827 29:171-180.
- 828 Davidson AJ, Yamazaki S, Arble DM, Menaker M, and Block GD (2008) Resetting of central and
- 829 peripheral circadian oscillators in aged rats. *Neurobiol Aging* 29:471-477.
- 830 Destici E, Jacobs EH, Tamanini F, Loos M, van der Horst GTJ, Oklejewicz M (2013) Altered phase-
- 831 relationship between peripheral oscillators and environmental time in *Cry1* or *Cry2* deficient mouse
- 832 models for early and late chronotypes. *PLoS ONE* 8, e83802.
- 833 Evans JA and Davidson AJ (2013) Health consequences of circadian disruption in humans and animal
- 834 models. *Prog Mol Biol Transl Sci* 119:283-323.
- 835 Evans JA, Leise TL, Castanon-Cervantes O, and Davidson AJ (2013) Dynamic interactions mediated by
- 836 nonredundant signaling mechanisms couple circadian clock neurons. *Neuron* 80:973-983.
- 837 Evans JA, Leise TL, Castanon-Cervantes O, and Davidson AJ (2011) Intrinsic regulation of
- 838 spatiotemporal organization within the suprachiasmatic nucleus. *PLoS One* 6:e15869.
- 839 Evans MS, Chaurette JP, Adams ST, Reddy GR, Paley MA, Aronin N, Prescher JA, and Miller SC (2014) A
- 840 synthetic luciferin improves bioluminescence imaging in live mice. *Nat Methods* 11:393-395.

- 841 Fonjallaz P, Ossipow V, Wanner G, and Schibler U (1996) The two PAR leucine zipper proteins, TEF  
842 and DBP, display similar circadian and tissue-specific expression, but have different target promoter  
843 preferences. *EMBO J* 15:351-362.
- 844 Goyal V, DeVera C, Baba K, Sellers J, Chrenek MA, Iuvone PM, Tosini G (2021) Photoreceptor  
845 degeneration in homozygous male *Per2<sup>luc</sup>* mice during aging. *J Biol Rhythms* 36:137-145.
- 846 Hamada T, Sutherland K, Ishikawa M, Miyamoto N, Honma S, Shirato H, and Honma K (2016) *In vivo*  
847 imaging of clock gene expression in multiple tissues of freely moving mice. *Nat Commun* 7:11705.
- 848 Hara R, Wan K, Wakamatsu H, Aida R, Moriya T, Akiyama M, and Shibata S (2001) Restricted feeding  
849 entrains liver clock without participation of the suprachiasmatic nucleus. *Genes Cells* 6:269-278.
- 850 Harris JA, Hirokawa KE, Sorensen SA, Gu H, Mills M, Ng LL, Bohn P, Mortrud M, Ouellette B, Kidney  
851 J, Smith KA, Dang C, Sunkin S, Bernard A, Oh SW, Madisen L, and Zeng H (2014) Anatomical  
852 characterization of Cre driver mice for neural circuit mapping and manipulation. *Front Neural*  
853 *Circuits* 8:76.
- 854 Herzog ED hermanstynne T, Smyllie NJ, Hastings MH (2017) Regulating the suprachiasmatic nucleus  
855 (SCN) clockwork: Interplay between cell-autonomous and circuit-level mechanisms. *Cold Springs*  
856 *Harbor Perspect Biol* 9: a027706.
- 857 Hirota T, Lee JW, Lewis WG, Zhang EE, Breton G, Liu X, Garcia M, Peters EC, Etchegaray JP, Traver  
858 D, Schulz PG, Kay SA (2010) High-throughput chemical screen identified a novel potent modulator  
859 of cellular circadian rhythms and reveals CK1 alpha as a clock regulatory kinase. *PLoS Biol* 8,  
860 e1000559
- 861 Iwano S, Sugiyama M, Hama H, Watakabe A, Hasegawa N, Kuchimaru T, Tanaka KZ, Takahashi M, Ishida  
862 Y, Hata J, Shimozono S, Namiki K, Fukano T, Kiyama M, Okano H, Kizaka-Kondoh S, McHugh TJ,  
863 Yamamori T, Hioki H, Maki S, and Miyawaki A (2018) Single-cell bioluminescence imaging of deep  
864 tissue in freely moving animals. *Science* 359:935-939.
- 865 Joye DAM, Rohr KE, Keller D, Inda T, Telega A, Pancholi H, Carmona-Alcocer V, and Evans JA (2020)  
866 Reduced VIP expression affects circadian clock function in VIP-IRES-CRE Mice (JAX 010908). *J*  
867 *Biol Rhythms* 35:340-352.
- 868 Kim JH, Lee SR, Li LH, Park HJ, Park JH, Lee KY, Kim MK, Shin BA, Choi SY. (2011) High cleavage  
869 efficiency of a 2A peptide derived from porcine Teschovirus-1 in human cell lines, zebrafish and  
870 mice. *PLoS ONE* 6, e18556
- 871 Kondo T, Strayer CA, Kulkarni RD, Taylor W, Ishiura M, Golden SS, and Johnson CH (1993) Circadian  
872 rhythms in prokaryotes: luciferase as a reporter of circadian gene expression in cyanobacteria. *Proc*  
873 *Natl Acad Sci U S A* 90:5672-5676.
- 874 Lee IT, Chang AS, Manandhar M, Shan Y, Fan J, Izumo M, Ikeda Y, Motoike T, Dixon S, Seinfeld JE,  
875 Takahashi JS, and Yanagisawa M (2015) Neuromedin S-producing neurons act as essential  
876 pacemakers in the suprachiasmatic nucleus to couple clock neurons and dictate circadian rhythms.  
877 *Neuron* 85:1086-1102.
- 878 Leise TL (2017) Analysis of nonstationary time series for biological rhythms research. *J Biol Rhythms*  
879 32:187-194.

- 880 Leise TL, Goldberg A, Michael J, Montoya G, Solow S, Molyneux P, Vetrivelan R, and Harrington ME  
881 (2020) Recurring circadian disruption alters circadian clock sensitivity to resetting. *Eur J Neurosci*  
882 51:2343-2354.
- 883 Leise TL and Harrington ME (2011) Wavelet-based time series analysis of circadian rhythms. *J Biol*  
884 *Rhythms* 26:454-463.
- 885 Leise TL, Harrington ME, Molyneux PC, Song I, Queenan H, Zimmerman E, Lall GS, and Biello SM  
886 (2013) Voluntary exercise can strengthen the circadian system in aged mice. *Age (Dordr)* 35:2137-  
887 2152.
- 888 Logan M, Martin JF, Nagy A, Lobe C, Olson EN, and Tabin CJ (2002) Expression of Cre recombinase in  
889 the developing mouse limb bud driven by a Prxl enhancer. *Genesis* 33:77-80.
- 890 Lopez-Molina L, Conquet F, Dubois-Dauphin M, and Schibler U (1997) The DBP gene is expressed  
891 according to a circadian rhythm in the suprachiasmatic nucleus and influences circadian behavior.  
892 *EMBO J* 16:6762-6771.
- 893 Martin-Burgos B, Wang W, William I, Tir S, Mohammad I, Javed R, Smith S, Cui Y, Smith CB, van  
894 der Vinne V, Molyneux PC, Miller SC, Weaver DR, Leise TL, Harrington ME (2020) Methods for  
895 detecting PER2::LUCIFERASE bioluminescence rhythms in freely moving mice. *BioRxiv*  
896 <https://doi.org/10.1038/s41467-017-00462-2>.
- 897 Maywood ES, Drynan L, Chesham JE, Edwards MD, Dardente H, Fustin JM, Hazlerigg DG, O'Neill JS,  
898 Codner GF, Smyllie NJ, Brancaccio M, and Hastings MH (2013) Analysis of core circadian feedback  
899 loop in suprachiasmatic nucleus of *mCry1-luc* transgenic reporter mouse. *Proc Natl Acad Sci U S A*  
900 110:9547-9552.
- 901  
902 Mei L, Fan Y, Lv X, Welsh DK, Zhan C, and Zhang EE (2018) Long-term in vivo recording of circadian  
903 rhythms in brains of freely moving mice. *Proc Natl Acad Sci U S A* 115:4276-4281.
- 904  
905 Mieda M, Okamoto H, and Sakurai T (2016) Manipulating the cellular circadian period of arginine  
906 vasopressin neurons alters the behavioral circadian period. *Curr Biol* 26:2535-2542.
- 907  
908 Mieda M, Ono D, Hasegawa E, Okamoto H, Honma K, Honma S, and Sakurai T (2015) Cellular clocks  
909 in AVP neurons of the SCN are critical for interneuronal coupling regulating circadian behavior  
rhythm. *Neuron* 85:1103-1116.
- 910  
911 Millar AJ, Short SR, Chua NH, and Kay SA (1992) A novel circadian phenotype based on firefly  
luciferase expression in transgenic plants. *Plant Cell* 4:1075-1087.
- 912  
913 Millar AJ, Carre IA, Strayer CA, Chua NH, Kay SA (1995). Circadian clock mutants in *Arabidopsis*  
identified by luciferase imaging. *Science* 267:1161-1163.
- 914  
915 Miller JE, Granados-Fuentes D, Wang T, Marpegan L, Holy TE, and Herzog ED (2014) Vasoactive  
916 intestinal polypeptide mediates circadian rhythms in mammalian olfactory bulb and olfaction. *J*  
*Neurosci* 34:6040-6046.
- 917  
918 Mohawk JA, Green CB, and Takahashi JS (2012) Central and peripheral circadian clocks in mammals.  
*Annu Rev Neurosci* 35:445-462.
- 919  
920 Morgan LW, Greene AV, and Bell-Pedersen D (2003) Circadian and light-induced expression of  
luciferase in *Neurospora crassa*. *Fungal Genet Biol* 38:327-332.

- 921 Muñoz-Guzmán F, Caballero V, and Larrondo LF (2021) A global search for novel transcription factors  
922 impacting the *Neurospora crassa* circadian clock. *G3* (Bethesda). DOI: 10.1093/g3journal/jkab100
- 923 Nagano M, Adachi A, Nakahama K, Nakamura T, Tamada M, Meyer-Bernstein E, Sehgal A, and  
924 Shigeyoshi Y (2003) An abrupt shift in the day/night cycle causes desynchrony in the mammalian  
925 circadian center. *J Neurosci* 23:6141-6151.
- 926 Nagoshi E, Saini C, Bauer C, Laroche T, Naef F, and Schibler U (2004) Circadian gene expression in  
927 individual fibroblasts: cell-autonomous and self-sustained oscillators pass time to daughter cells. *Cell*  
928 119:693-705.
- 929 Nakamura W, Yamazaki S, Takasu NN, Mishima K, and Block GD (2005) Differential response of  
930 *Period 1* expression within the suprachiasmatic nucleus. *J Neurosci* 25:5481-5487.
- 931 Nakamura W, Yamazaki S, Nakamura TJ, Shirakawa T, Block GD, and Takumi T (2008) *In vivo*  
932 monitoring of circadian timing in freely moving mice. *Curr Biol* 18:381-385.
- 933 Nicholls SK, Casiraghi LP, Wang W, Weber ET, and Harrington ME (2019) Evidence for internal  
934 desynchrony caused by circadian clock resetting. *Yale J Biol Med* 92:259-270.
- 935 Noguchi T, Harrison EM, Sun J, May D, Ng A, Welsh DK, and Gorman MR (2020) Circadian rhythm  
936 bifurcation induces flexible phase resetting by reducing circadian amplitude. *Eur J Neurosci* 51:2329-  
937 2342.
- 938 Ono D, Honma K, and Honma S (2015a) Circadian and ultradian rhythms of clock gene expression in the  
939 suprachiasmatic nucleus of freely moving mice. *Sci Rep* 5:12310.
- 940 Patke A, Young MW, and Axelrod S (2020) Molecular mechanisms and physiological importance of  
941 circadian rhythms. *Nat Rev Mol Cell Biol* 21:67-84.
- 942 Pezuk P, Mohawk JA, Wang LA, and Menaker M (2012) Glucocorticoids as entraining signals for  
943 peripheral circadian oscillators. *Endocrinology* 153:4775-4783.
- 944 Postic C, Shiota M, Niswender KD, Jetton TL, Chen Y, Moates JM, Shelton KD, Lindner J, Cherrington  
945 AD, and Magnuson MA (1999) Dual roles for glucokinase in glucose homeostasis as determined by  
946 liver and pancreatic beta cell-specific gene knock-outs using Cre recombinase. *J Biol Chem* 274:305-  
947 315.
- 948 Poulsen RC, Warman GR, Sleight J, Ludin NM, and Cheeseman JF (2018) How does general anaesthesia  
949 affect the circadian clock? *Sleep Med Rev* 37:35-44.
- 950 Punia S, Rumery KK, Yu EA, Lambert CM, Notkins AL, and Weaver DR (2012) Disruption of gene  
951 expression rhythms in mice lacking secretory vesicle proteins IA-2 and IA-2 $\beta$ . *Am J Physiol*  
952 *Endocrinol Metab* 303:762.
- 953 Ralph MR, Shi SQ, Johnson CH, Houdek P, Shrestha TC, Crosby P, O'Neill JS, Sladek M, Stinchcombe  
954 AR, and Sumova A (2021) Targeted modification of the *Per2* clock gene alters circadian function in  
955 *mPer2<sup>luciferase</sup> (mPer2<sup>Luc</sup>)* mice. *PLoS Comput Biol* 17:e1008987.
- 956 Reddy AB, Field MD, Maywood ES, and Hastings MH (2002) Differential resynchronisation of circadian  
957 clock gene expression within the suprachiasmatic nuclei of mice subjected to experimental jet lag. *J*  
958 *Neurosci* 22:7326-7330.

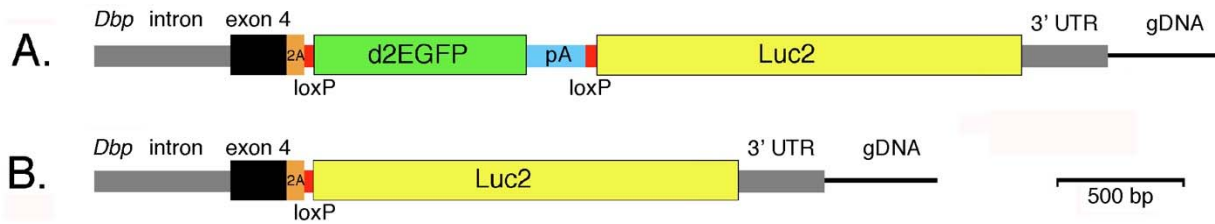
- 959 Ripperger JA and Schibler U (2006) Rhythmic CLOCK-BMAL1 binding to multiple E-box motifs drives  
960 circadian *Dbp* transcription and chromatin transitions. *Nat Genet* 38:369-374.
- 961 Roenneberg T and Merrow M (2016) The Circadian Clock and Human Health. *Curr Biol* 26:432.
- 962 Saini C, Liani A, Curie T, Gos P, Kreppel F, Emmenegger Y, Bonacina L, Wolf JP, Poget YA, Franken  
963 P, and Schibler U (2013) Real-time recording of circadian liver gene expression in freely moving  
964 mice reveals the phase-setting behavior of hepatocyte clocks. *Genes Dev* 27:1526-1536.
- 965 Sawai Y, Okamoto T, Muranaka Y, Nakamura R, Matsumura R, Node K, and Akashi M (2019) *In vivo*  
966 evaluation of the effect of lithium on peripheral circadian clocks by real-time monitoring of clock gene  
967 expression in near-freely moving mice. *Sci Rep* 9:10909-3.
- 968 Sellix MT, Evans JA, Leise TL, Castanon-Cervantes O, Hill DD, DeLisser P, Block GD, Menaker M, and  
969 Davidson AJ (2012) Aging differentially affects the re-entrainment response of central and peripheral  
970 circadian oscillators. *J Neurosci* 32:16193-16202.
- 971 Shan Y, Abel JH, Li Y, Izumo M, Cox KH, Jeong B, Yoo SH, Olson DP, Doyle FJ, and Takahashi JS  
972 (2020) Dual-color single-cell imaging of the Suprachiasmatic Nucleus reveals a circadian role in  
973 network synchrony. *Neuron* 108:164-179.e7
- 974 Shao X; Somlo S; Igarashi P (2002) Epithelial-specific Cre/lox recombination in the developing kidney  
975 and genitourinary tract. *J Am Soc Nephrol* 13: 1837-1846.
- 976 Sinturel F, Gos P, Petrenko V, Hagedorn C, Kreppel F, Storch KF, Knutti D, Liani A, Weitz C,  
977 Emmenegger Y, Franken P, Bonacina L, Dibner C, and Schibler U (2021) Circadian hepatocyte  
978 clocks keep synchrony in the absence of a master pacemaker in the suprachiasmatic nucleus or other  
979 extrahepatic clocks. *Genes Dev* 35:329-334.
- 980 Stanewsky R, Kaneko M, Emery P, Beretta B, Wager-Smith K, Kay SA, Rosbash M, and Hall JC (1998)  
981 The *cry<sup>b</sup>* mutation identifies cryptochrome as a circadian photoreceptor in *Drosophila*. *Cell* 95:681-  
982 692.
- 983 Stokkan KA, Yamazaki S, Tei H, Sakaki Y, and Menaker M (2001) Entrainment of the circadian clock in  
984 the liver by feeding. *Science* 291:490-493.
- 985 Stratmann M, Suter DM, Molina N, Naef F, and Schibler U (2012) Circadian *Dbp* transcription relies on  
986 highly dynamic BMAL1-CLOCK interaction with E boxes and requires the proteasome. *Mol Cell*  
987 48:277-287.
- 988 Tahara Y, Kuroda H, Saito K, Nakajima Y, Kubo Y, Ohnishi N, Seo Y, Otsuka M, Fuse Y, Ohura Y,  
989 Komatsu T, Moriya Y, Okada S, Furutani N, Hirao A, Horikawa K, Kudo T, and Shibata S (2012) *In*  
990 *vivo* monitoring of peripheral circadian clocks in the mouse. *Curr Biol* 22:1029-1034.
- 991 van der Vinne V, Martin Burgos B, Harrington ME, and Weaver DR (2020) Deconstructing circadian  
992 disruption: Assessing the contribution of reduced peripheral oscillator amplitude on obesity and  
993 glucose intolerance in mice. *J Pineal Res* 69:e12654.
- 994 van der Vinne V, Swoap SJ, Vajtay TJ, and Weaver DR (2018) Desynchrony between brain and  
995 peripheral clocks caused by CK1 $\delta/\epsilon$  disruption in GABA neurons does not lead to adverse metabolic  
996 outcomes. *Proc Natl Acad Sci U S A* 115:E2437-E2446.

- 997 Weaver DR, van der Vinne V, Giannaris EL, Vajtay TJ, Holloway KL, and Anaclet C (2018)  
998 Functionally complete excision of conditional alleles in the mouse suprachiasmatic nucleus by *Vgat-*  
999 *IRE5-Cre*. *J Biol Rhythms* 33:179-191.
- 1000 Weger M, Weger BD, Diotel N, Rastegar S, Hirota T, Kay SA, Strahle U, and Dickmeis T (2013) Real-  
1001 time *in vivo* monitoring of circadian E-box enhancer activity: a robust and sensitive zebrafish reporter  
1002 line for developmental, chemical and neural biology of the circadian clock. *Dev Biol* 380:259-273.
- 1003 Welsh DK, Yoo SH, Liu AC, Takahashi JS, Kay SA (2004) Bioluminescence imaging of individual  
1004 fibroblasts reveals persistent, independently phased circadian rhythms of clock gene expression. *Curr*  
1005 *Biol* 14:2289-2295.
- 1006 West AC and Bechtold DA (2015) The cost of circadian desynchrony: Evidence, insights and open  
1007 questions. *Bioessays* 37:777-788.
- 1008 Xie X, Kukino A, Calcagno HE, Berman AM, Garner JP, and Butler MP (2020) Natural food intake  
1009 patterns have little synchronizing effect on peripheral circadian clocks. *BMC Biol* 18:160-7.
- 1010 Yamaguchi S, Kobayashi M, Mitsui S, Ishida Y, van der Horst, G. T., Suzuki M, Shibata S, and Okamura  
1011 H (2001) View of a mouse clock gene ticking. *Nature* 409:684.
- 1012 Yamaguchi Y, Suzuki T, Mizoro Y, Kori H, Okada K, Chen Y, Fustin JM, Yamazaki F, Mizuguchi N,  
1013 Zhang J, Dong X, Tsujimoto G, Okuno Y, Doi M, and Okamura H (2013) Mice genetically deficient  
1014 in vasopressin V1a and V1b receptors are resistant to jet lag. *Science* 342:85-90.
- 1015 Yamaguchi Y, Okada K, Mizuno T, Ota T, Yamada H, Doi M, Kobayashi M, Tei H, Shigeyoshi Y,  
1016 Okamura H (2016). Real-time recording of circadian *Per1* and *Per2* expression in the  
1017 suprachiasmatic nucleus of freely moving rats. *J Biol Rhythms* 31:108-111.
- 1018 Yamanaka Y, Honma S, and Honma K (2008) Scheduled exposures to a novel environment with a  
1019 running-wheel differentially accelerate re-entrainment of mice peripheral clocks to new light-dark  
1020 cycles. *Genes Cells* 13:497-507.
- 1021 Yamazaki S and Takahashi JS (2005) Real-time luminescence reporting of circadian gene expression in  
1022 mammals. *Methods Enzymol* 393:288-301.
- 1023 Yamazaki S, Numano R, Abe M, Hida A, Takahashi R, Ueda M, Block GD, Sakaki Y, Menaker M, and  
1024 Tei H (2000) Resetting central and peripheral circadian oscillators in transgenic rats. *Science*  
1025 288:682-685.
- 1026 Yoo SH, Ko CH, Lowrey PL, Buhr ED, Song EJ, Chang S, Yoo OJ, Yamazaki S, Lee C, and Takahashi  
1027 JS (2005) A noncanonical E-box enhancer drives mouse *Period2* circadian oscillations *in vivo*. *Proc*  
1028 *Natl Acad Sci U S A* 102:2608-2613.
- 1029 Yoo SH, Yamazaki S, Lowrey PL, Shimomura K, Ko CH, Buhr ED, Siepkas SM, Hong HK, Oh WJ, Yoo  
1030 OJ, Menaker M, and Takahashi JS (2004) PERIOD2::LUCIFERASE real-time reporting of circadian  
1031 dynamics reveals persistent circadian oscillations in mouse peripheral tissues. *Proc Natl Acad Sci U S*  
1032 *A* 101:5339-5346.
- 1033 Yoo SH, Kojima S, Shimomura K, Koike N, Buhr ED, Furukawa T, Ko CH, Glostom G, Ayoub C,  
1034 Nohara K, Reyes BA, Tsuchiya Y, Yoo OJ, Yagita K, Lee C, Chen Z, Yamazaki S, Green CB, and  
1035 Takahashi JS (2017) *Period2* 3'-UTR and microRNA-24 regulate circadian rhythms by repressing  
1036 PERIOD2 protein accumulation. *Proc Natl Acad Sci U S A* 114:E8855-E8864.

- 1037 Zhang EE, Liu AC, Hirota T, miraglia LJ, Welch G, Pongsawakul PY, liu X, Atwood A, Huss JW 3<sup>rd</sup>,  
1038 Janes J, Su AI, Hogenesch JB, Kay SA (2009) A genome-wide RNAi screen for modulators of the  
1039 circadian clock in human cells Cell 139: 199-210.
- 1040 Zhang R, Lahens NF, Ballance HI, Hughes ME, and Hogenesch JB (2014) A circadian gene expression  
1041 atlas in mammals: implications for biology and medicine. Proc Natl Acad Sci U S A 111:16219-  
1042 16224.
- 1043

1044 **Figures and Tables**

1045



1046

1047 **Figure 1. Generation of a bifunctional reporter from the mouse *Dbp* locus.**

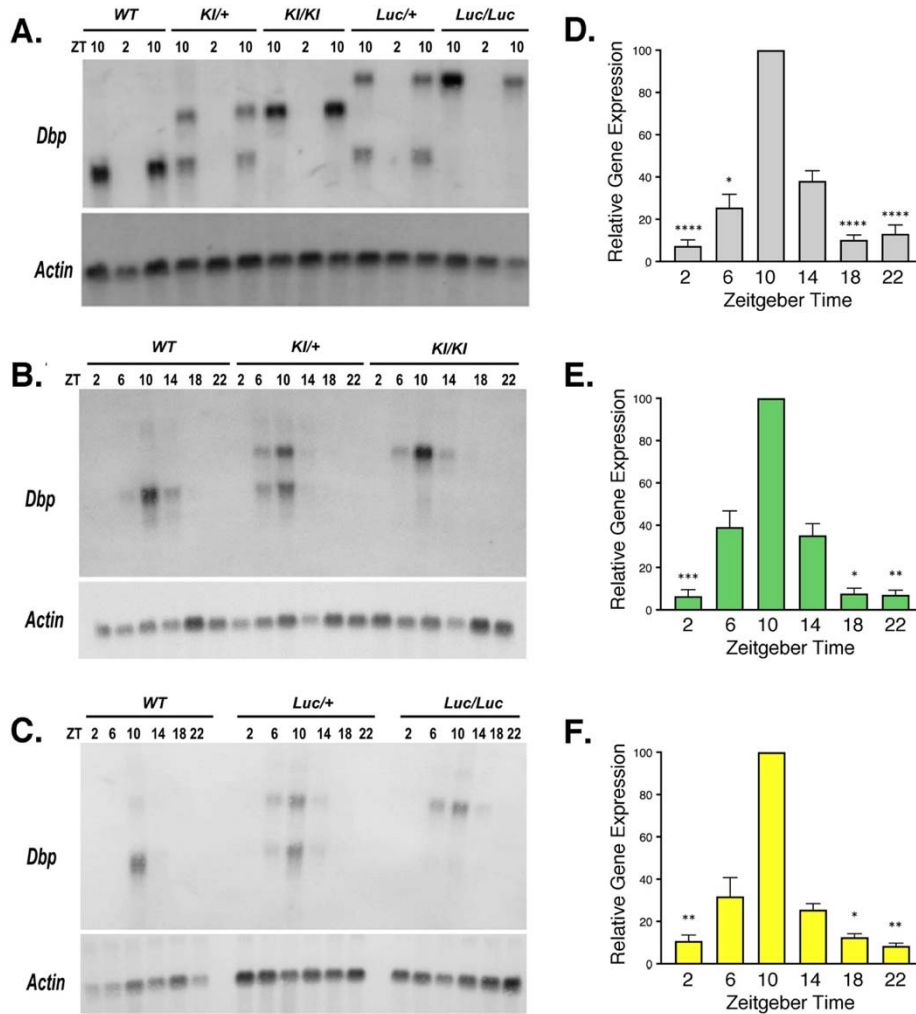
1048 **A.** The mouse *Dbp* locus was modified by CRISPR-mediated insertion of the donor construct shown. The  
1049 construct contained homology arms from the *Dbp* locus (gray and black) and inserted the reporter  
1050 sequences with a T2A-encoding sequence (orange) between DBP and the reporter. Destabilized EGFP  
1051 (d2EGFP) with a bovine growth hormone polyadenylation site (PA) was flanked by *loxP* sites (red).  
1052 Downstream of *GFP* is a luciferase (*Luc2*) reporter gene. Without recombination *Dbp* and *GFP* are  
1053 expressed as a single transcript from the conditional (*Dbp*<sup>KI</sup> allele).

1054 **B.** With *Cre*-mediated recombination, GFP-encoding sequences are excised and *Dbp* and *luciferase* are  
1055 expressed as a single transcript. The T2A sequence generates separate proteins from these bifunctional  
1056 transcripts. *Cre*-mediated germline recombination led to mice expressing luciferase non-conditionally  
1057 from the *Dbp*<sup>Luc</sup> allele.

1058

1059





1060

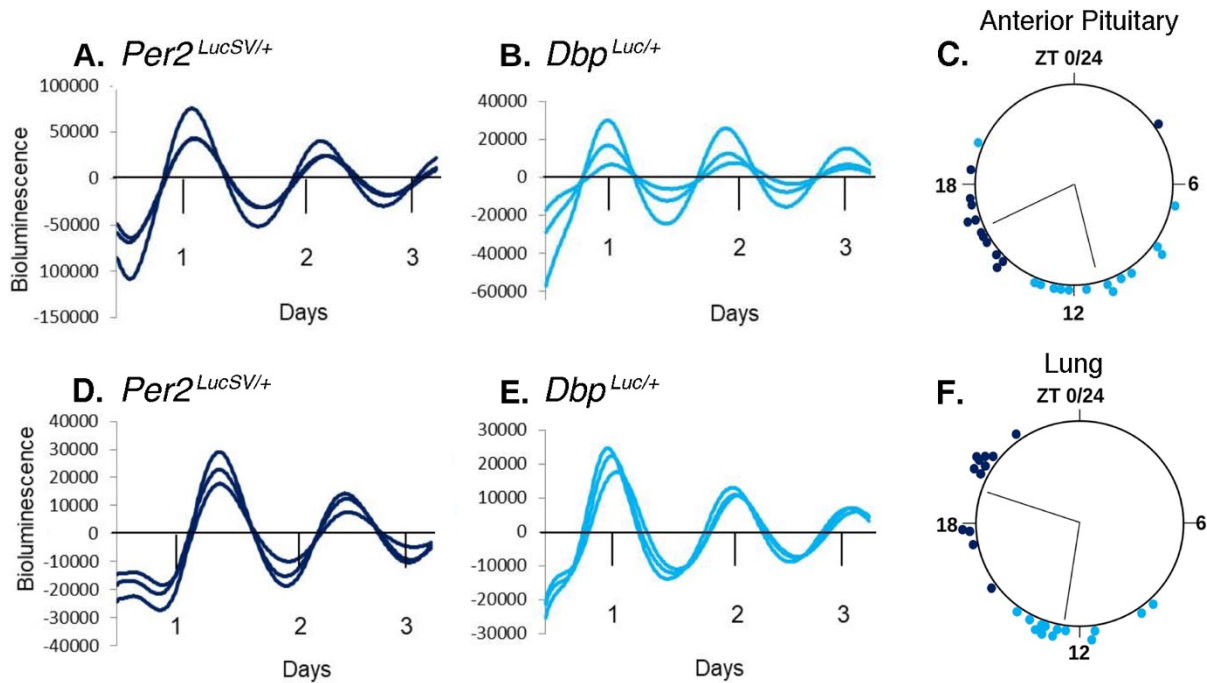
1061 **Figure 2. *Dbp* mRNA rhythms are not altered in reporter mice**

1062 **A-C.** Representative Northern Blots probed to detect *Dbp* and *Actin* mRNA. **A.** From each of five  
 1063 genotypes, RNA samples were extracted from livers collected at ZT 2 and 10. For each genotype, there  
 1064 are two samples at ZT10 and one sample at ZT2 on this blot. **B.** and **C.** Representative Northern Blots of  
 1065 RNA samples collected from WT and reporter mouse livers at each of six Zeitgeber times (ZT).

1066 **D-F.** Quantification of *Dbp* mRNA rhythms for each allele in time-series experiments (6 time-points  
 1067 each). Results are expressed as mean ( $\pm$  SEM) percent of the peak *Dbp/Actin* ratio, which occurred at ZT  
 1068 10 on every blot. **D.** Wild-type *Dbp* transcript (n=12 sample sets). **E.** *Dbp<sup>KI</sup>* transcript (n= 6). **F.** *Dbp<sup>Luc</sup>*  
 1069 transcript (n= 6). For each transcript, there was a significant rhythm (Friedman's One-way ANOVA,  $Q >$   
 1070 19,  $p < 0.002$ ). Asterisks indicate time-points that differed significantly from ZT10 (Dunn's test, \*  $p <$   
 1071 0.05, \*\*  $p < 0.01$ , \*\*\*  $p < 0.001$ , \*\*\*\*  $p \leq 0.0001$ ). Significant differences among some other time-points  
 1072 are not shown for clarity.

1073

1074



1075

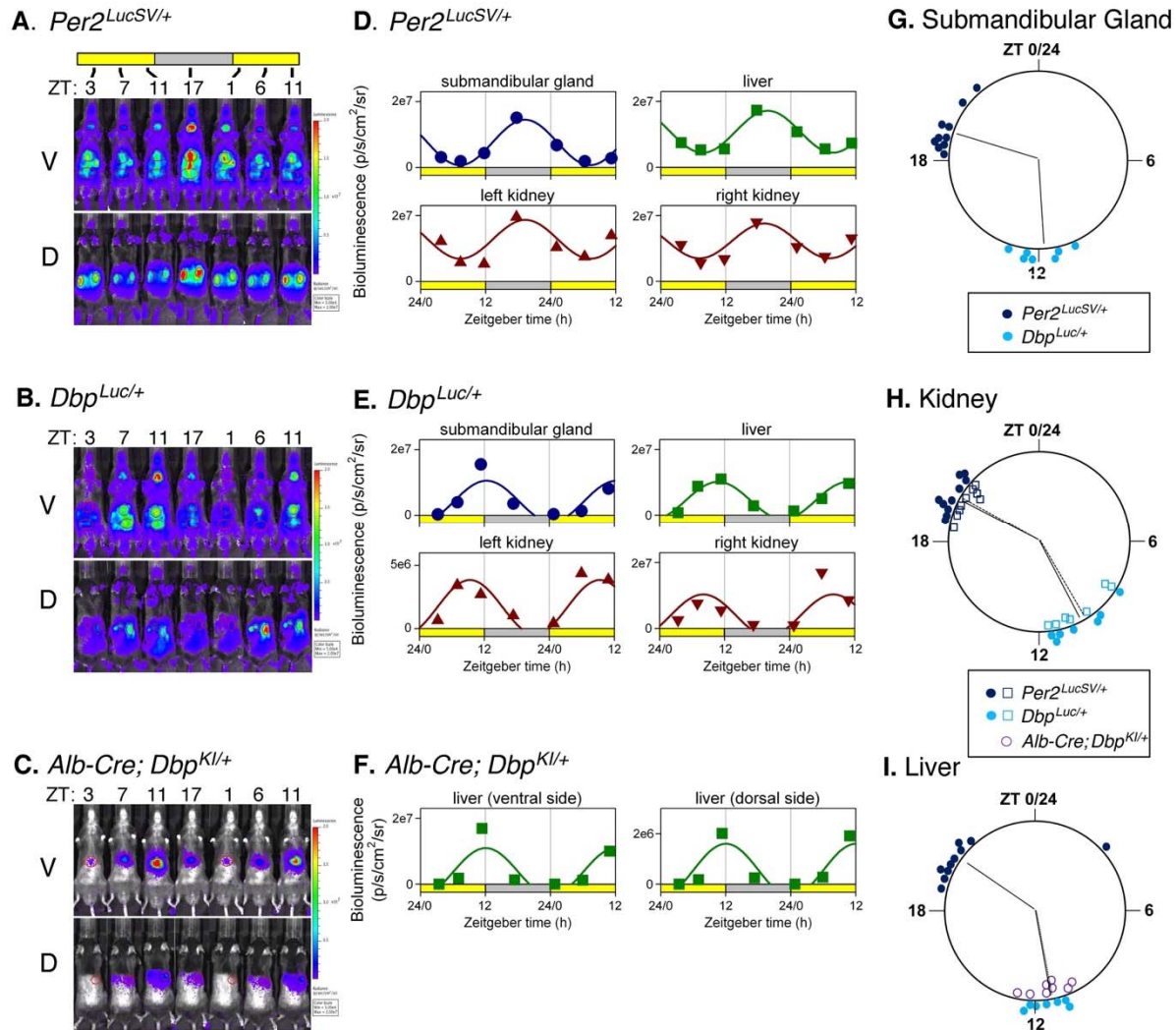
1076 **Figure 3. Ex vivo bioluminescence rhythms from *Per2<sup>LucSV/+</sup>* and tissue explants.**

1077 **A-C, Anterior Pituitary gland. D-F, Lung.**

1078 **A., B., D., and E.** are representative bioluminescence rhythms from triplicate tissue explants from  
1079 *Per2<sup>LucSV/+</sup>* (**A, D**) and *Dbp<sup>Luc/+</sup>* mice (**B, E**). ‘Days’ refers to time in culture, not projected ZT. Values are  
1080 24-h background-subtracted and 3-h smoothed.

1081 **C, F.** Time of peak bioluminescence *ex vivo*. The large circles represent a 24-h day for each organ. ZT’s  
1082 refer to the lighting cycle to which the mice were exposed prior to sample collection, with ZT0-12 being  
1083 the light phase. Colored circles at the perimeter of the large circle indicate the timing of peak  
1084 bioluminescence of individual *Per2<sup>LucSV/+</sup>* (dark blue) or *Dbp<sup>Luc/+</sup>* (teal) tissue explants (n=12-14 mice).  
1085 Within each tissue/genotype combination, there was significant clustering of times of peak  
1086 bioluminescence. Radial lines represent the mean peak time, which differed significantly between  
1087 genotypes for each tissue (Watson-Williams test, p<0.001).

1088



1089

1090 **Figure 4. Bioluminescence rhythms measured *in vivo***

1091 **A-C.** Bioluminescence images captured at 4-6 hr intervals from a representative mouse of each genotype.

1092 **A.** *Per2<sup>LucSV/+</sup>*, **B.** *Dbp<sup>Luc/+</sup>* **C.** *Alb-Cre<sup>+</sup>; Dbp<sup>KI/+</sup>*. Ventral (V) and dorsal (D) views are shown for each

1093 mouse. All images for each mouse are set to the same luminescence scale.

1094 **D-F.** Cosinor-fitting of bioluminescence signal over time for the animals shown in Panels A-C to

1095 determine peak time. Bioluminescence rhythms were assessed in submandibular gland, liver, and kidneys

1096 of **(D.)** *Per2<sup>LucSV/+</sup>* and **(E.)** *Dbp<sup>Luc/+</sup>* reporter mice, and from liver of *Alb-Cre<sup>+</sup>; Dbp<sup>KI/+</sup>* mice **(F.)**.

1097 **G-I.** Time of peak bioluminescence *in vivo*. **G.** Submandibular gland, **H.** Kidneys, and **I.** Liver. Data

1098 plotted as in Fig. 3. *Per2<sup>LucSV/+</sup>* tissues (n=10, dark blue), *Dbp<sup>Luc/+</sup>* tissues (n=7, teal). In Panel H, open

1099 squares and filled circles represent the right and left kidneys, respectively. In Panel I, purple circles

1100 represent livers from *Alb-Cre<sup>+</sup>; Dbp<sup>KI/+</sup>* mice (n=8). Radial lines represent the mean peak time for each

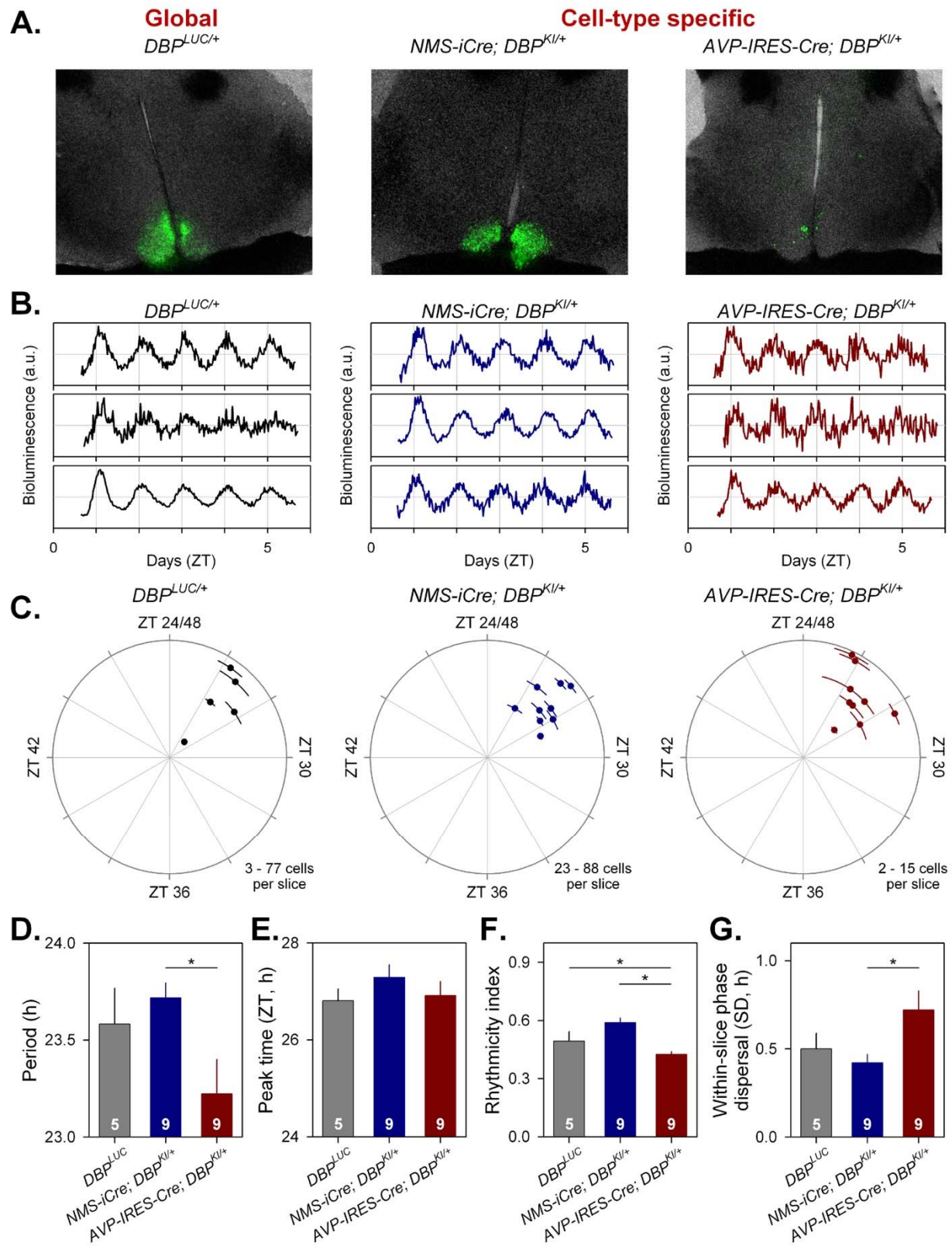
1101 genotype and tissue. Radial lines from the two kidneys of a genotype are nearly overlapping. For liver,

1102 radial lines for the two *Dbp* reporter lines are overlapping and appear as a single line. Within each organ  
1103 examined, time of peak differed significantly in *Per2<sup>LucSV/+</sup>* explants compared to *Dbp<sup>Luc/+</sup>* and *Alb-Cre+* ;  
1104 *Dbp<sup>KI/+</sup>* explants ( $p=0.002$ , Watson-Williams test). There was no significant difference in peak time  
1105 between *Dbp<sup>Luc/+</sup>* and *Alb-Cre+* ; *Dbp<sup>KI/+</sup>* liver tissues ( $p>0.05$ ).

1106

1107

1108

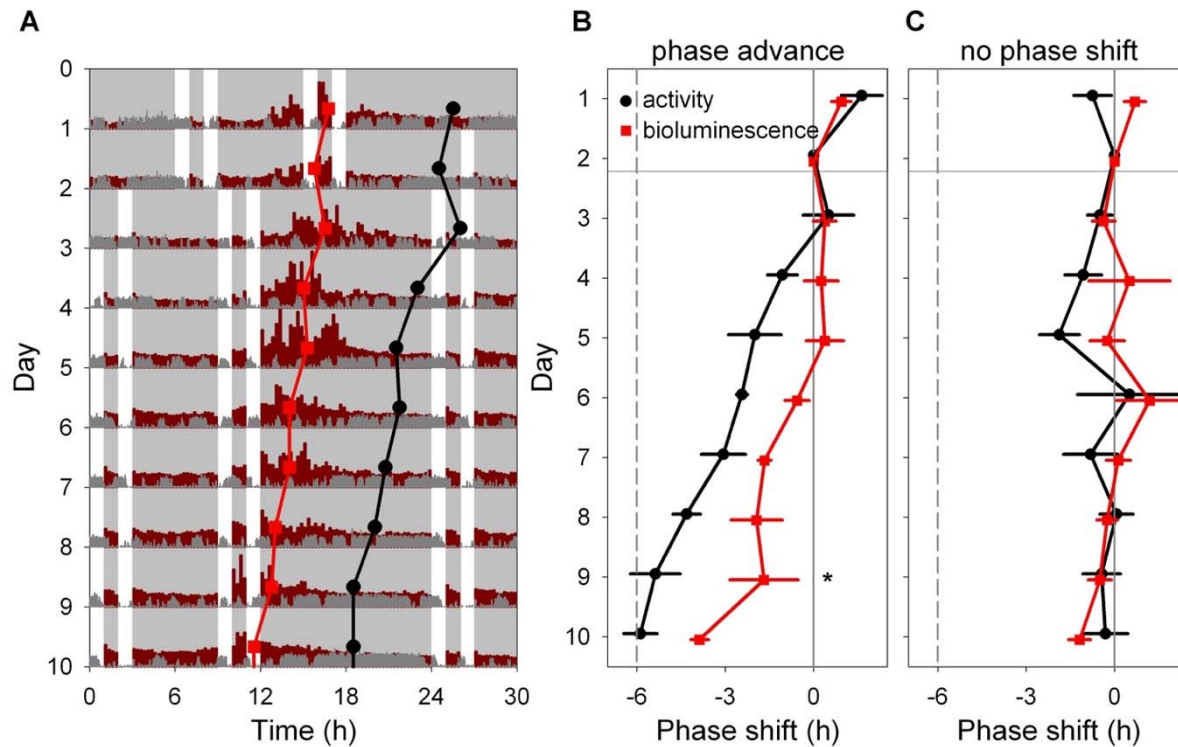


1109

1110

**Figure 5. Cell-type-specific imaging of luciferase expression in SCN slices**

1111  
1112 **A)** 24h summed bioluminescence overlaid onto bright field images of a section through the SCN from  
1113 *Dbp<sup>Luc/+</sup>* (global reporter expression, left), and in mice expressing luciferase from specific subsets of SCN  
1114 neurons (NMS<sup>+</sup> cells, center; AVP<sup>+</sup> cells, right).  
1115 **B.** Representative bioluminescence traces from single neuron-like ROIs in slices from each genotype.  
1116 **C.** Circular plots indicate the peak time of bioluminescence rhythms from each genotype. Time is  
1117 expressed relative to the light-dark cycle the mice were housed in prior to sacrifice; numbers >24 are used  
1118 to indicate that these measures are recorded on the first day in culture and are plotted relative to the  
1119 previous lighting conditions. Each slice is represented by a small dot. Placement of the dot relative to  
1120 outer circle indicates average peak time ( $\pm$ SD), while the distance from the center corresponds to the  
1121 number of cells incorporated in the average ( $\sqrt{\text{cell\#}}$ ).  
1122 **D-G.** Rhythm parameters by genotype. The number of slices per genotype is indicated at the base of each  
1123 bar.  
1124 **D.** Mean period ( $\pm$  SEM).  
1125 **E.** Circular mean peak time ( $\pm$  SEM).  
1126 **F.** Mean rhythmicity index score ( $\pm$  SEM).  
1127 **G.** Mean peak time dispersal (quantified by circular SD of peak times within each slice).  
1128  
1129



1130

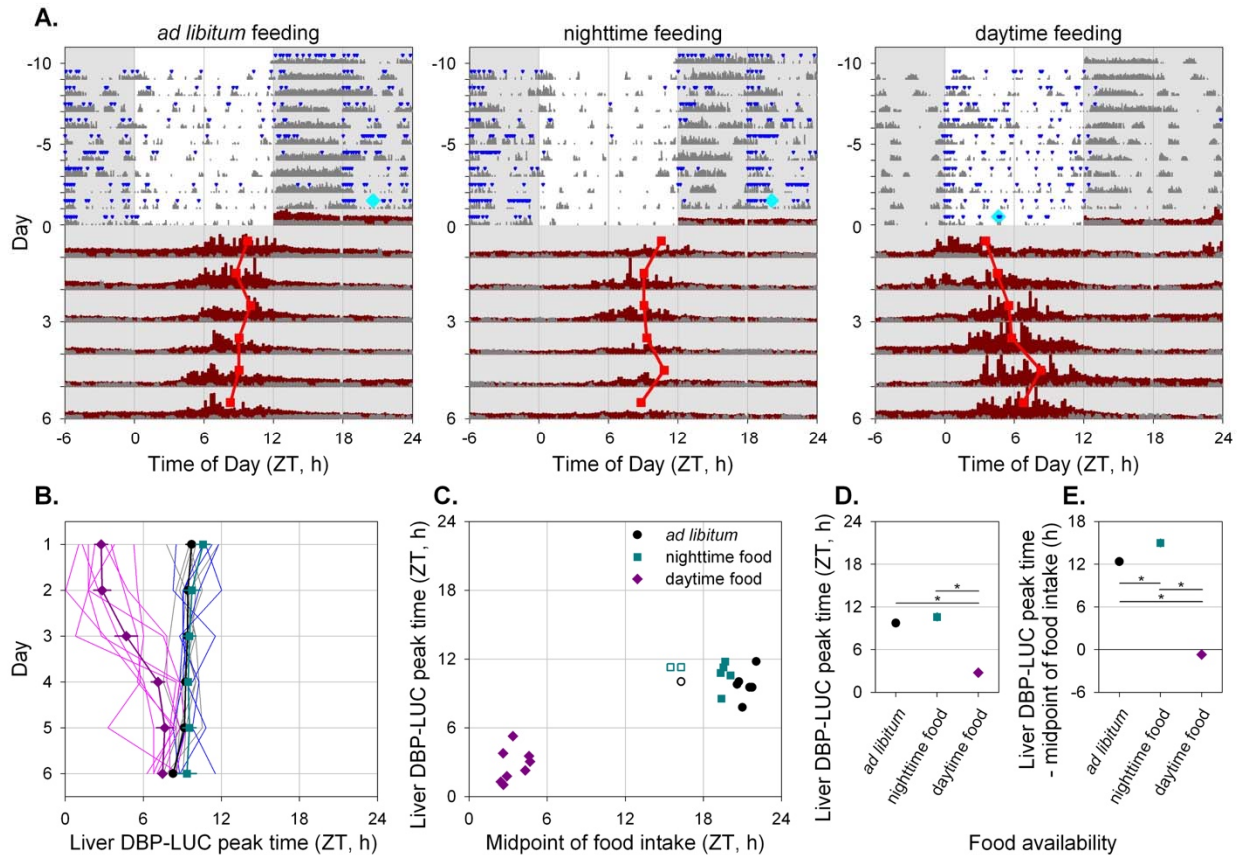
1131 **Figure 6. Light-induced resetting produces misalignment between rhythms in liver**  
1132 **bioluminescence and locomotor activity.**

1133 **A.** Representative double-plotted actogram showing locomotor activity (dark gray) and bioluminescence  
1134 (dark red) of an *Alb-Cre; Dbp<sup>KI/+</sup>* liver reporter mouse before and after a 6-h advance of the skeleton  
1135 photoperiod consisting of four 1-h periods of light per 24-h day, as indicated by white. The skeleton  
1136 photoperiod was advanced by 6 h by shortening the dark phase after the last light pulse on Day 2. Red  
1137 squares represent the peak of the bioluminescence rhythm, while black circles represent the midpoint of  
1138 locomotor activity each day, determined by discrete wavelet transform analysis. Six hours of each cycle  
1139 are double-plotted to aid visualization. Light and dark are indicated by white and gray backgrounds,  
1140 respectively.

1141 **B.** Mean ( $\pm$  SEM) midpoint of locomotor activity (black) and peak of liver bioluminescence (red) rhythms  
1142 are shown, relative to their initial value, in a group of 4 mice exposed to a 6-h phase advance of the  
1143 skeleton photoperiod. The locomotor activity rhythm re-sets more rapidly than the bioluminescence  
1144 rhythm within animal (Significant Measure \* Day interaction, and significant phase difference between  
1145 the rhythms on Day 9; Tukey HSD,  $p < 0.05$ ).

1146 **C.** Mean ( $\pm$  SEM) time of midpoint of locomotor activity (black) and peak liver bioluminescence (red)  
1147 rhythms are shown, relative to their initial phase, in a group of 4 mice not subjected to a phase shift of the  
1148 skeleton photoperiod.

1149



1150

1151 **Figure 7. Time-restricted feeding alters the timing of liver bioluminescence rhythms.**

1152 **A.** Representative actograms of three *Alb-Cre; Dbp<sup>KI/+</sup>* liver reporter mice exposed to the different  
 1153 feeding regimes as indicated above each panel. Mice were housed in 12L:12D lighting and exposed  
 1154 to the specified feeding regime for ten days (-10 to 0) before bioluminescence recording. Food  
 1155 intake (blue triangles) and general locomotor activity (dark gray) were recorded continuously. The  
 1156 midpoint of food intake from days -5 to 0 is indicated by a cyan diamond on day 0. Mice were  
 1157 transferred to the bioluminescence recording setup at the start of the dark phase and housed in  
 1158 constant darkness with *ad libitum* food access. Liver bioluminescence levels are depicted in dark  
 1159 red. Red squares represent the time of peak of the bioluminescence rhythm, determined by DWT.  
 1160 Six hours of each cycle are double-plotted and the y-axis has been stretched during the last 6 days  
 1161 to aid visualization. Light and dark are indicated by white and gray backgrounds, respectively.

1162 **B.** Individual and mean ( $\pm$  SEM) phase of liver bioluminescence rhythms relative to clock time for  
 1163 three feeding groups. Mice previously exposed to *ad libitum*, nighttime and daytime feeding are  
 1164 plotted in grey/black, blue/cyan and magenta, respectively (key in Panel C). Prior to recording  
 1165 bioluminescence, mice were entrained to a 12L:12D lighting cycle with lights on at 0600. Mice



- 1166 previously exposed to daytime feeding show an advanced peak phase of liver bioluminescence that  
1167 reverts over time in constant darkness with *ad libitum* food.
- 1168 **C.** Relationship between preceding feeding phase and peak liver bioluminescence phase for individual  
1169 animals on the first day under constant conditions. *Ad libitum* and night-fed groups had similar  
1170 midpoint of food intake; three “outliers” with respect to midpoint of food intake (shown by open  
1171 symbols) were not included in further analyses (Panels B, D and E).
- 1172 **D.** Mean ( $\pm$  SEM) peak liver bioluminescence phase on the first day under constant conditions, relative  
1173 to clock time for the three feeding regimens. Error bars were nearly or completely contained within  
1174 the symbols.
- 1175 **E.** Mean ( $\pm$ SEM) peak liver bioluminescence phase on the first day under constant conditions, relative  
1176 to the midpoint of preceding food intake for the three feeding regimens. Error bars were nearly or  
1177 completely contained within the symbols.
- 1178

1179 **Table 1:** Period length of locomotor activity rhythms in constant darkness, by sex and genotype

1180

1181	Genotype	Sex	N	$\tau_{DD}$ (Mean $\pm$ SEM), h
1182	<i>Dbp</i> <sup>+/+</sup>	Male	15	23.88 $\pm$ 0.027
1183	<i>Dbp</i> <sup>KI/+</sup>	Male	10	23.91 $\pm$ 0.057
1184	<i>Dbp</i> <sup>KI/KI</sup>	Male	11	23.92 $\pm$ 0.036
1185	<i>Dbp</i> <sup>Luc/+</sup>	Male	11	23.86 $\pm$ 0.025
1186	<i>Dbp</i> <sup>Luc/Luc</sup>	Male	8	23.97 $\pm$ 0.029
1187				
1188	<i>Dbp</i> <sup>+/+</sup>	Female	21	23.87 $\pm$ 0.021
1189	<i>Dbp</i> <sup>KI/+</sup>	Female	9	23.89 $\pm$ 0.036
1190	<i>Dbp</i> <sup>KI/KI</sup>	Female	11	23.79 $\pm$ 0.030
1191	<i>Dbp</i> <sup>Luc/+</sup>	Female	8	23.82 $\pm$ 0.053
1192	<i>Dbp</i> <sup>Luc/Luc</sup>	Female	8	23.75 $\pm$ 0.042